Assessment of Mitochondrial Dysfunction in Lungs from Rats Exposed to Hyperoxia and the Efficacy of Duroquinone

Swetha Ganesh
Marquette University

ASSESSMENT OF MITOCHONDRIAL DYSFUNCTION IN LUNGS FROM RATS EXPOSED TO HYPEROXIA AND THE EFFICACY OF DUROQUINONE

By

Swetha Ganesh, B.S.

A thesis submitted to the Faculty of the Graduate School, Marquette University, in Partial Fulfillment of the Requirements for the Degree of Master of Science

Milwaukee, Wisconsin

December 2021

ABSTRACT

ASSESSMENT OF MITOCHONDRIAL DYSFUNCTION IN LUNGS FROM RATS EXPOSED TO HYPEROXIA AND THE EFFICACY OF DUROQUINONE

Swetha Ganesh, B.S.

Marquette University,2021

Dissipation of mitochondrial membrane potential ($\Delta\psi_m$) is a hallmark of mitochondrial dysfunction. The objective of this thesis was to use a previously developed experimental-computational approach to estimate tissue $\Delta\psi_m$ in intact lungs of rats exposed to hyperoxia, and to evaluate the ability of duroquinone (DQ) to reverse any hyperoxia-induced depolarization of lung $\Delta\psi_m$. Rats were exposed to hyperoxia (>95% O_2) or normoxia (room air) for 48 hrs, after which lungs were excised and connected to a ventilation-perfusion system. The experimental protocol consisted of measuring the concentration of the fluorescent dye rhodamine 6G (R6G) during three single-pass phases: loading, washing, and uncoupling, in which the lungs were perfused with and without R6G, and with the mitochondrial uncoupler FCCP, respectively. For normoxic lungs, the protocol was repeated with 1) rotenone (complex I inhibitor), 2) rotenone and either DQ or its vehicle (DMSO), and 3) rotenone, glutathione (GSH), and either DQ or DMSO added to the perfusate. Hyperoxic lungs were studied with and without DQ and GSH added to the perfusate. Computational modeling was used to estimate lung $\Delta\psi_m$ from R6G data. The results show that rat exposure to hyperoxia caused a partial depolarization (−38 mV) of lung $\Delta\psi_m$, and complex I inhibition depolarized lung $\Delta\psi_m$ by −90 mV. Results also demonstrate the efficacy of DQ to fully reverse both rotenone-induced and hyperoxia-induced lung $\Delta\psi_m$ depolarization. This study demonstrates hyperoxia-induced $\Delta\psi_m$ depolarization in intact lungs, and the utility of this approach for assessing the impact of potential therapies such as exogenous quinones that target mitochondria in intact lung.

ACKNOWLEDGEMENTS

Swetha Ganesh, B.S.

First and foremost, I would like to express my sincere gratitude to Dr. Said Audi who has been an ideal teacher, mentor, and thesis supervisor. I want to express my genuine appreciation for his patience and understanding through it all.

Also, I would like to give a sincere thanks to Dr. Anne Clough, Dr. Elizabeth Jacobs, and Dr. Ranjan Dash for serving on this thesis committee and for their encouragement and insightful comments.

I would also like to thank Pardis Taheri, who has been a constant source of support and encouragement during the challenges of graduate school and life. I am truly thankful for having you in my life.

My deep and sincere gratitude to my family for their continuous and unparalleled love, help and support. I am extremely grateful to my sister for being my best friend and for always inspiring me through every step of my life. I am forever indebted to my mom and dad for giving me the opportunities and experiences that have made me who I am today.

I dedicate my thesis to my partner and my support system, Chandi, who has always been my biggest motivation. Thanks for your understanding, your never-ending encouragement, and for always being there for me. Your support has meant more to me than you could possibly realize.

Lastly, I want to thank Marquette University for giving me the opportunity to earn my master's degree and to work on this project. I extend my heartfelt gratitude to all those who have contributed, directly and indirectly, to the completion of this thesis.

TABLE OF CONTENTS

LIST OF TABLES

LIST OF FIGURES

CHAPTER 1: INTRODUCTION, BACKGROUND, AND OBJECTIVE

1.1 Clinical Motivation

Acute lung injury (ALI) and its most severe form acute respiratory distress syndrome (ARDS) are characterized by rapidly progressing hypoxic lung failure and carry high morbidity and mortality rates (Laffey & Matthay, 2017). ALI/ARDS can be initiated by direct or indirect injury to the lung (Matthay et al., 2019). Direct injury to the lungs can be caused by pneumonia, inhalation of harmful chemicals, pulmonary tissue injury, and indirect injury can be caused by sepsis, multiple blood transfusions and severe trauma (Matthay et al., 2003)(Matthay et al., 2012). Direct or indirect injury to the lungs can in turn lead to inflammation and oxidative stress which affect the bronchial epithelium, alveolar macrophages, and vascular endothelium and disrupts the air-blood barrier leading to a protein-rich fluid accumulation in the alveoli. This in turn impairs the vital gas exchange function of the lungs, which in many cases can lead to multi-organ failure and death (Han et al., 2015).

The high morbidity and mortality rates of ARDS are to a large extent due to the lack of effective therapies (Matthay et al., 2003). Current therapies are mostly limited to supplemental supportive care. This includes low tidal volume protective ventilation, prone positioning, and conservative fluid management (Levitt et al., 2012). However, mechanical ventilation can lead to lung inflammation and ventilator-induced lung injury (Kellner et al., 2017). Studies using prophylactic aspirin, inhaled nitric oxide, mesenchymal stem cells, and intravenous β-agonists have not shown much mortality benefit (Ma et al., 2019). Furthering our understanding of the pathogenesis of ALI could lead to the identification of potential therapeutic targets.

Studies have shown that ARDS development could be in part due to dysfunction of mitochondria bioenergetic of lungs (Cloonan et al., 2020)(Ten & Ratner, 2020). Lung cellular mitochondria produce ~80-90% of the required ATP for the normal functioning of cells (Fisher, 1984) (Bagkos et al., 2014). The mitochondrial membrane potential ($\Delta\Psi_m$) is a major component of the proton motive force that drives the synthesis of ATP at mitochondrial complex V and controls the rate of respiration and the generation of reactive oxygen species (ROS) (Zorova et al., 2018). Thus, a change in the $\Delta\Psi_m$ is an indicator of mitochondrial dysfunction in lung cells (Audi et al., 2020).

Fluorescent lipophilic cationic dyes have been used to probe $\Delta\Psi_m$ mainly in cultured cells and isolated mitochondria (Perry et al., 2011)(Scaduto & Grotyohann, 1999)(Gan et al., 2011)(Wolken & Arriaga, 2014)(Adrie et al., 2001). A small number of studies have used these dyes to probe $\Delta\Psi_m$ in intact functioning organs (Audi et al., 2020; Hough et al., n.d.; Sakamuru et al., 2016; Scaduto & Grotyohann, 1999). Recently, Audi et al. developed an experimental-computational approach for estimating $\Delta\Psi_m$ in millivolts (mV) in isolated perfused rat lungs using the cationic rhodamine dye rhodamine 6G (R6G) (Audi et al., 2020). The *objective* of my thesis is to use this approach to assess $\Delta\Psi_m$ in intact lungs from rats exposed to hyperoxia (> 95% O_2 for 48 hours) as a model of human ALI, and to evaluate the ability of the ubiquinone analog duroquinone to reverse any hyperoxia-induced depolarization of $\Delta\Psi_m$ (Audi et al., 2003, 2005).

1.2 Role of mitochondria in lung cellular functions: ATP Production

The mitochondrion is a multifunctional organelle which plays an important role in cellular ATP synthesis, redox homeostasis, apoptosis, and intracellular energy transfer

(Zorov et al., 2014). Figure 1 shows the key processes of oxidative phosphorylation (with glucose as substrate) which takes place in mitochondria and is responsible for 80-90% of ATP production in lung cells. This process begins with the cellular uptake of glucose, which is the major substrate for lung cells under physiological conditions (Fisher, 1984). Following its uptake, glucose is phosphorylated to glucose-6-phosphate which then enters glycolysis resulting in the conversion of a glucose molecule to two molecules of pyruvate. Pyruvate from glycolysis goes into the mitochondrial matrix and is converted into a two-carbon molecule bound to Coenzyme A, known as acetyl CoA. Acetyl CoA is a molecule that is further converted to oxaloacetate, which enters the citric acid cycle (Krebs cycle) where it undergoes oxidation and generates electron donors such as NADH and $FADH_2$. The electrons are then transferred to the electron transport chain (ETC) to reduce molecular O_2 to H_2O at complex IV and in the process undergo multiple redox reactions that result in the pumping of H^+ from the matrix to the intermembrane space at complexes I, III and IV, creating a proton motive force that drives the production of ATP from ADP and inorganic phosphate at complex V. $\Delta\Psi_m$ is an important component of this proton motive force.

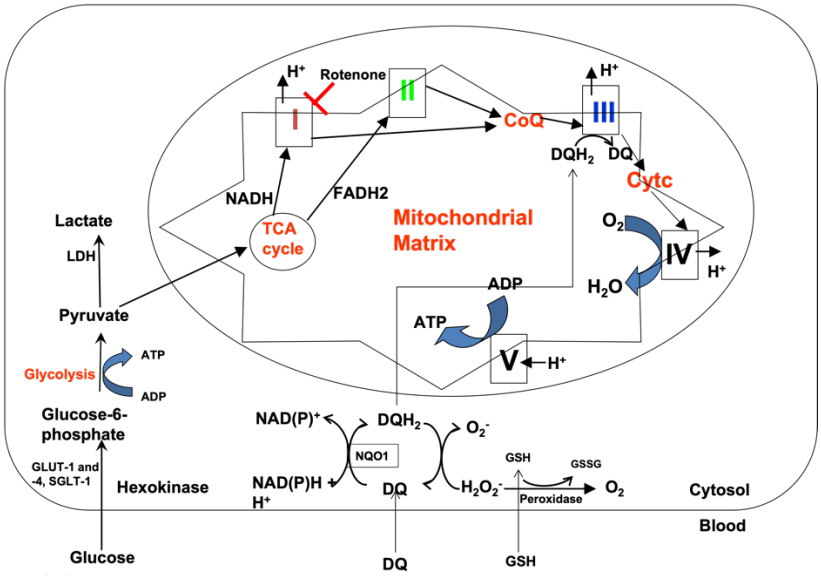

***Figure* 1:** *ATP is generated by oxidative phosphorylation in the inner mitochondrial membrane conducted by the four complexes of the ETC and ATP synthase (Complex V). Inhibition sites of the mitochondrial complex I by rotenone are represented by red blunted arrows. G6PD catalyzes $NADP^+$ to its reduced form, NADPH, in the pentose phosphate pathway. Abbreviations: G6PD=Glucose-6-phosphate dehydrogenase; ATP=Adenosine triphosphate; ADP=Adenosine diphosphate; NADP+=Nicotinamide adenine dinucleotide phosphate [oxidized form]; NADPH=Reduced NADP; GSSG=Oxidized glutathione; GSH=Reduced glutathione ; CytC =Cytochrome C; CoQ = Coenzyme Q ; LDH = Lactate dehydrogenase*

1.3 Rat exposure to hyperoxia as a model of human ALI:

Several rodent models of human ALI/ARDS have been developed (Kallet & Matthay, 2013)(Crapo et al., 1980)(Sepehr et al., 2013)(Audi et al., 2005). Rat exposure to hyperoxia (>95% O_2) is a well-established animal model of human ALI/ARDS (Sepehr et al., 2013)(Bassett et al., 1992)(Crapo et al., 1980)(Audi et al., 2017). This model reproduces the cardinal features of clinical ALI/ARDS, namely bilateral lung infiltration, decreased lung compliance, parenchyma injury including increased vascular permeability, low-pressure edema, and hypoxemia (Matute-Bello et al., 2008)(Crapo et al., 1980)(Levitt & Matthay, 2012).

Crapo et al. studied the structural and biochemical changes in lungs from rats following exposure to 100% O_2 until death (Crapo et al., 1980). They showed that in comparison to rats exposed to room air, no significant anatomical changes were seen in the lungs of rats exposed to 100% O_2 for up to 40 hours. By 60 hours, however, there was a 30% loss in pulmonary capillary endothelial cells and cell surface, lung infiltration of phagocytic leukocytes and other cells, and an increase in air-blood barrier thickness by 56%. Rats that survived 60 hours of 100% O_2 exposure lost 44% of their pulmonary capillary endothelial cells and developed edema, which results in the thickening of the air-blood barrier, pleural effusion, severe hypoxemia, and eventually death within 72 hours (Crapo et al., 1980).

1.4 Mitochondrial changes in lungs of rodents exposed to hyperoxia as a model of human ALI:

Inflammation, oxidative stress, and mitochondrial dysfunction has been shown to play key roles in the pathogenesis of hyperoxia-induced ALI (Liu et al., 2017) (Liu X, 2017). Previous studies have reported hyperoxia-induced mitochondrial changes in lung tissue/cells early in the pathogenesis of hyperoxia-induced ALI (Audi et al., 2005)(Gan et al., 2011)(Merker et al., 2006)(Merker et al., 2007)(Sepehr et al., 2013). Sepehr et al. reported ~77% decrease in lung tissue complex I activity per mg protein from rats exposed to hyperoxia (>95% O_2 for 48 hrs) (Sepehr et al., 2013). In the same study, they showed using surface fluorometry that rat exposure to hyperoxia decreased rotenone-induced change in NADH signal by 63%, as an index of lung tissue complex I activity, as compared to that of normoxic lungs. In addition to decrease in lung tissue complex I activity, Sepehr et al. reported a 63% decrease in mitochondrial complex II activity in lung tissue from rats exposed to >95% O_2 for 48 hours as compared to that from lungs of

normoxic rats, and a 56% decrease in lung surface FAD signal in the presence of potassium cyanide (complex IV inhibitor) and pentachlorophenol (mitochondrial uncoupler), as an index of lung complex II activity. Based on these results, they concluded that the lung tissue electron transport chain (ETC) upstream from complexes I and II is more reduced in intact hyperoxic lungs than in normoxic lungs, and that activities of complexes I and II are lower in hyperoxic lungs as compared to normoxic lungs (Sepehr et al., 2013).

The above-mentioned decreases in mitochondrial complex I and II activities following exposure to hyperoxia (> 95% O_2 for 48 hours) would be expected to alter the proton motive force and partially depolarize $\Delta\psi_m$, which in turn could alter mitochondria bioenergetics and respiration. This is consistent with results from Audi et al. in which they quantified $\Delta\psi_m$ of isolated mitochondria from normoxic and hyperoxic lungs using the cationic dye rhodamine 123 (R123) (Audi et al., 2017). For this preparation, the addition of ADP (state 3) in the presence of the complex I substrates, pyruvate + malate, or complex II substrate, succinate, stimulated transient and reversible efflux of R123 from the mitochondria and is consistent with partial depolarization of $\Delta\psi_m$. One measure of the kinetics of ADP-stimulated $\Delta\psi_m$ depolarization is the full width half maximum time (FWHM) for R123 to return to the baseline (state 2). Audi et al. showed that rat exposure to hyperoxia (>95% O_2 for 48 hours) increased FWHM by 67% and 60% in the presence of the complex I substates (pyruvate + malate) and complex II substrate (succinate), respectively. This suggests that $\Delta\psi_m$ recovery from ADP-induced depolarization in mitochondria from hyperoxic lungs was substantially slower than that in

normoxic lungs, consistent with decreases in lung tissue complex I (79%) and II (64%) activities with hyperoxia (Sepehr et al., 2013).

Das et al. showed that exposure of mice to 90% O_2 for 48 hours decreased the activities of lung tissue complexes I and II, as well as basal, state 3 and uncoupled state 3 respiratory rates in isolated mitochondria (Das, 2013). They also determined complex IV activity using ascorbate and concluded that hyperoxia does not affect complex IV (Das, 2013).

Fisher AB showed that rat exposure to 95% O_2 for 48 hours had no effect on total lung tissue ATP content as compared to normoxic lungs (Fisher, 1978). However, rats exposed to hyperoxia (95% O_2 for 48 hours) increased the lactate to pyruvate ratio in lungs, which was measured as an indicator of the lung rate of ATP synthesis via the glycolytic pathway. Lung lactate production rate increased by 61%, whereas as lung rate of pyruvate production decreased by ~8% which led to doubling of the lactate/pyruvate ratio. Based on these results, they concluded that hyperoxia-induced increase in glycolytic ATP production could compensate for decrease in ATP production via oxidative phosphorylation and that the increased lactate-to pyruvate ratio was in response to decreased mitochondrial ATP synthesis (Fisher, 1978).

Bassett et al. showed no effect on FAD-linked metabolism in mitochondria isolated from lungs of rats exposed to hyperoxia (100% O_2 for 24 hours) (Bassett et al., 1992). However, in the presence of NAD-linked substrates, respiratory rates were significantly reduced. They showed that baseline and ADP-stimulated mitochondrial respiratory rates were significantly lower in the presence of NAD-linked substrates for mitochondria from lungs of hyperoxia-exposed rats as compared to normoxia (room air)

exposed rats (Bassett et al., 1992). These results are consistent with a hyperoxia-induced decrease in complex I early in the pathogenesis of hyperoxia-induced ALI.

Gan et al quantified the mitochondrial and plasma membrane potential in cultured bovine pulmonary endothelial cells (BPECs) using the rhodamine dye R123 and TMRE in control and hyperoxia (95% O_2 for 48 hours) exposed cells by measuring the dynamic dye concentrations in the medium (Gan et al., 2011). They showed that $\Delta\Psi_m$ in hyperoxia-exposed cells are more sensitive to depolarization by a mitochondrial uncoupler than $\Delta\Psi_m$ in normoxia-exposed cells, consistent with hyperoxia-induced mitochondrial deficiency in BPECs (Gan et al., 2011).

Beyer et al. performed western analyses on rat lung homogenates from normoxic and hyperoxia lungs using an antibody cocktail containing antibodies to each of the five mitochondrial complexes and showed clear bands consistent with complexes I through V in all samples. They showed (Figure 2) that the expressions of complexes I and II were significantly lower in lungs samples from hyperoxia rats (Beyer et al., 2021). Hyperoxia had no significant effects on the expressions of complexes III, IV and V.

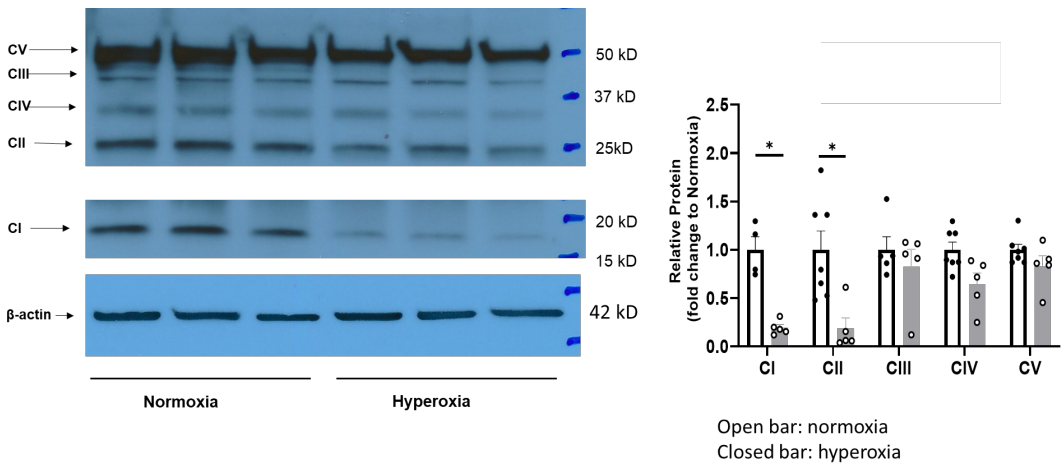

***Figure 2**: Representative western blots (left) and summary of results (right) of the expressions of complexes I, II, III, IV and V in lung samples from normoxic and hyperoxic rats (Beyer et al., 2021). *different from normoxia ($p < 0.05$)*

1.5 Mitochondrial membrane potential, oxidative stress, and mitochondrial dysfunction

$\Delta\Psi_m$ is an important component of the proton motive force that is generated via complexes I, III, and IV of the electron transport chain. The proton gradient and the $\Delta\Psi_m$ together drive the production of ATP at complex V. The direction of the $\Delta\Psi_m$ drives the inward transport of cations and outward transport of anions. The accumulation of cations in the mitochondria depends on $\Delta\Psi_m$, which also plays a key role in transporting other ions (other than H^+) to ensure healthy functioning of mitochondria and the elimination of disabled mitochondria. Normally, $\Delta\Psi_m$ and ATP production rates are stable. However, sustained changes in the $\Delta\Psi_m$ and in turn in cellular ATP production are considered indicators of various pathologies which are depicted by either depolarized or hyperpolarized $\Delta\Psi_m$. A depolarized $\Delta\Psi_m$ is potentially very harmful to cells since it reduces the production of ATP (Zorova et al., 2018).

$\Delta\Psi_m$ is a result of redox transformations that occur in the TCA cycle. It is an intermediary energy storage which is utilized by the ATP synthase (complex V) to

produce ATP and is the most reliable indicator of mitochondrial function (Zorova et al., 2018)(Bagkos et al., 2014). Various studies have shown that the range for $\Delta\Psi_m$ measured from the rat's lungs, heart, liver and cultured neurons is between -125 to -150 mV for maximum production of ATP (Bagkos et al., 2014)(Alpert et al., 2018)(Hassinen et al., 1984)(Wan et al., 1993)(Audi et al., 2020). Depolarization of $\Delta\Psi_m$, and thus lower ATP production rate, lead to mitochondrial dysfunction which is a key factor in the pathogenesis of ALI/ARDS (Bagkos et al., 2014)(Schumacker et al., 2014). Loss of lung air-blood barrier is caused in part by mitochondrial dysfunction which can lead to endothelial/epithelial cell death (Cloonan et al., 2020)(Levitt & Matthay, 2012). This in part can allow neutrophils to pass across the barrier and induce additional tissue damage by producing cytotoxic secretions (Mittal et al., 2014), such as ROS, pro-inflammatory cytokines, bioactive lipids, all important factors in the pathogenesis of ALI/ARDS (Kellner et al., 2017).

There are many sources of reactive oxygen species (ROS) in the cells, including NADPH oxidases (NOX), xanthine oxidase, and mitochondria (Kellner et al., 2017). In controlled quantities, ROS are critical in signaling growth, differentiation, progression (Zhang et al., 2016). Increased or uncontrolled ROS production by lung cells can lead to the disruption of the lung capillary endothelial barrier and alveolar epithelium increasing the vascular leakage resulting in pulmonary edema (Kellner et al., 2017).

The electrons in complex I donated from NADH are transported through the FMN (flavoprotein), Fe-S clusters and then to the ubiquinone Q. The ROS superoxide (O_2^-) is produced at each of these steps by complex I. Complex III produces O_2^- during the Q cycle, which is the transfer of electrons from complexes I and II to complex III and in

turn reduces ubiquinone to ubiquinol. Oxidation of ubiquinol donates two electrons to cytochrome c and results in an unstable ubisemiquinone and donates a single electron to O_2, generating O_2^- which gets converted to H_2O_2 within the mitochondria and diffuses to the cytoplasmic compartment. Hyperoxia-induced increase in ROS formation could damage the complex I activity by oxidizing the lipid cardiolipin, which is sensitive to ROS (Sepehr et al., 2013). Since complex II is encoded by nuclear DNA, damage to mDNA due to hyperoxia-induced increase in the rate of ROS formation should not affect complex II. However the apparent decrease in complex II activity could be a compensatory mechanism by the cells to reduce ROS formation under hyperoxic conditions (Sepehr et al., 2013). Damage to complex I and complex III can lead to significant decrease in mitochondrial ATP production.

An increase in ROS can produce extremely harmful effects and if not balanced by antioxidants, can lead to chronic inflammatory conditions (Pizzino et al., 2017). The imbalance in the oxidants and antioxidants produces oxidative stress. Glutathione (GSH) is an antioxidant which, in its reduced form, usually modulates the levels of ROS produced by donating a proton to neutralize H_2O_2 (Presnell et al., 2013). The ability to neutralize ROS depends on the GSH/GSSG concentration which decreases with oxidative stress (Aquilano et al., 2014). The mitochondria are one of the key sources of ROS generation which greatly depend on the $\Delta\Psi m$. Depolarization of $\Delta\Psi m$ can exponentially increase mitochondrial ROS production (Gao et al., 2008).

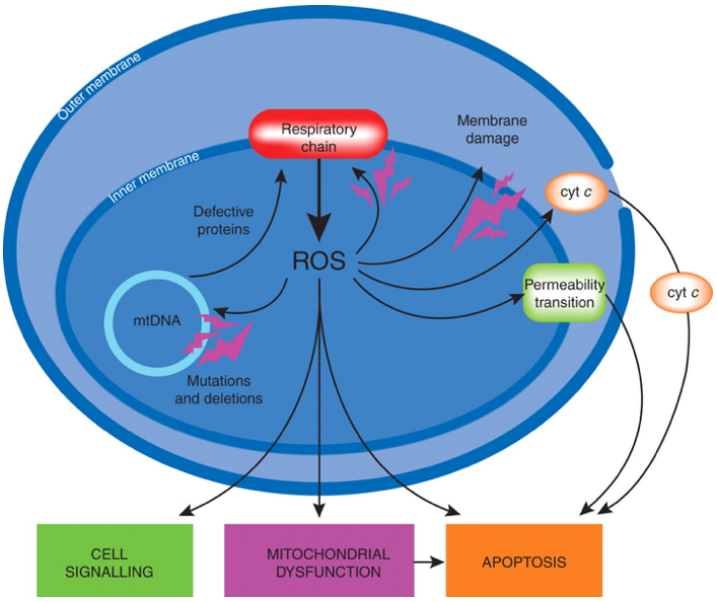

Figure 3: *The effect of ROS on the mitochondria affecting the ability of Mitochondria to produce ATP. Oxidative stress in the mitochondria releases cytochrome C into the cytosol and leads to apoptosis. It can also lead to membrane damage and increase the permeability making the inner membrane more permeable to small molecules. Mitochondrial ROS is also an important cell signaling pathway and modulates various cell functions (Galley, 2011).*

1.6 Methods to measure $\Delta\Psi_m$:

Various cationic fluorescence dyes have been used to assess $\Delta\Psi_m$ mostly in reduced systems, including isolated mitochondria or cultured cells (Perry et al., 2011)(Scaduto & Grotyohann, 1999)(Gan et al., 2011)(Adrie et al., 2001). Limited studies have attempted to measure $\Delta\Psi_m$ in intact functioning lungs (Sakamuru et al., 2016)(Hough et al., 2019) (Audi et al., 2020).

Arriaga et al. used the method of capillary electrophoresis with laser-induced fluorescence detection to measure $\Delta\Psi_m$ in isolated mitochondria from mouse liver and muscle cells (Arriaga et al., 2014). JC-1 was used as the fluorescence probe in isolated mitochondria and red/green fluorescence intensity ratios from individual mitochondria were used as an indicator of mitochondrial membrane potential (Arriaga et al., 2014).

However, the disadvantage of using JC-1 is that it is sensitive to factors other than the $\Delta\Psi_m$, such as surface/volume ratio due to aggregation (Perry et al., 2011).

Baraccaa et al. assessed mitochondrial respiration and membrane potential (bioenergetics) in isolated rat liver mitochondria using the dye rhodamine 123 (R123 (Baracca et al., 2003). Mitochondrial respiration was measured under four respiratory states. State 1 is the condition under which isolated mitochondria are added to the respiration buffer with no substrates. State 2 is the respiratory state following the addition of complex I substrates such as pyruvate and malate or complex II substates such as succinate to the respiration buffer. State 3 respiration is reached following the addition of high concentrations of ADP which is converted to ATP (Lanza & Nair, 2009). State 3 is characterized as the state with saturating ATP usage/production (Korzeniewski, 2015). State 4 is the respiratory state that is reached following the full conversion of added ADP to ATP (Lanza & Nair, 2009) (Korzeniewski, 2015). The uncoupled respiration is achieved by adding an uncoupler (FCCP) which causes dissipation of the proton gradient across the inner mitochondrial membrane. They showed that the dynamic and steady-state R123 redistribution across the inner mitochondrial membrane can be used to detect membrane potential changes by measuring the rate of fluorescence quenching (Baracca et al., 2003).

Johnson et al. used cationic fluorescence probes such as rhodamines B, 3B, 6G, 19, 110, 116, 123, and tetramethyl rhodamine, ANS, merocyanine 540 and fluorescein in a variety of living cells to monitor $\Delta\Psi_m$ using fluorescence microscopy (Johnson et al., 1981). The results show that differences in the intensity of mitochondrial-associated fluorescence can reflect the functional state of mitochondria. The variations in

mitochondrial membrane potential and the accumulation of the cationic compounds may be an indicator for increased ATP requirements (Johnson et al., 1981).

Gan et al. developed an experimental and computational approach for evaluating $\Delta\Psi_m$ and plasma membrane potential in cultured bovine pulmonary arterial endothelial cells. The study involved the addition of a rhodamine dye to the medium containing the cells and measuring the dye medium concentrations over time (Gan et al., 2011). They used computational modeling to estimate the values of $\Delta\Psi_m$ and plasma membrane potential (in mV) from the dynamic medium dye concentrations. Their results show that for cells exposed to hyperoxia (95% O_2 for 48 hours), their $\Delta\Psi_m$ is more sensitive to depolarization than control cells (exposed to room air) (Gan et al., 2011).

Scaduto et al. measured $\Delta\Psi_m$ in isolated perfused rat heart and isolated mitochondria from rat heart using the rhodamine cationic dye TMRM (Scaduto & Grotyohann, 1999). The $\Delta\Psi_m$ in isolated perfused heart was measured from the surface emission fluorescence of the dye. The fluorescence properties were found to change upon accumulation in the mitochondria causing a red shift in the wavelength which was used to measure $\Delta\Psi_m$ by fluorescence ratio method. However, they were not able to observe the spectral shift in the TMRM loaded rat heart due to accumulation of the dye in both mitochondria and the cytosol (Scaduto & Grotyohann, 1999) .

Hough et al. assessed the $\Delta\Psi_m$ in isolated intact mice lungs by inducing chemical injury with HCl using an alveolar micro puncture technique (Hough et al., 2019). They used confocal microscopy to measure the change in the fluorescence intensity from TMRE in microvascular endothelial cells as an index of $\Delta\Psi_m$, before and after inducing injury with HCl. The acid injection decreased the TMRE fluorescence indicating the

mitochondrial depolarization in the endothelial cells. This approach is limited to measuring the change in $\Delta\Psi_m$ in a localized lung region and therefore does not measure the overall change in $\Delta\Psi_m$ in the lungs (Hough et al., 2019).

Audi et al. developed an experimental and computational approach for measuring the $\Delta\Psi_m$ in intact functioning rat lungs (Audi et al., 2020). The approach involves measuring the concentration of cationic fluorescent dye rhodamine 6G (R6G) in the lung venous effluent following its infusion through the pulmonary artery. A physiological-based pharmacokinetic (PBPK) model of the pulmonary disposition of R6G was then used for quantitative interpretation of the data and for estimating the value of the lung $\Delta\Psi_m$ (in mV). The objective of this thesis is to make use of this approach to assess the effect of rat exposure to hyperoxia (>95% O_2 for 48 hours) as a model of clinical acute lung injury.

1.7 Potential utility of exogenous quinone compounds to reverse mitochondrial dysfunction due to decreases in complex I and/or II activities.

Previous studies assessed the disposition of the quinone compounds duroquinone (DQ) and coenzyme Q1 (CoQ1) in isolated perfused rat lungs and cultured pulmonary endothelial cells (Audi et al., 2003)(Audi et al., 2005)(Merker et al., 2004). They showed that the two-electron reduction of DQ to durohydroquinone (DQH_2) was predominantly via the cytosolic enzyme NAD(P)H quinone dehydrogenase 1 (NQO1), and that the oxidation of DQH_2 back to DQ is via mitochondrial complex III (Figure 3). For CoQ1, they showed that its two-electron reduction to coenzyme Q1 hydroquinone ($CoQ1H_2$) is via NQO1 and mitochondrial complex I, and that the oxidation of $CoQ1H_2$ is via mitochondrial complex III (Figure 3).

Previous studies in cultured bovine pulmonary endothelial cells reported hyperoxia-induced changes in the reduction rate of DQ to DQH_2 and CoQ1 to $CoQ1H_2$ (Merker et al., 2007)(Merker et al., 2006)(Audi et al., 2005). The results showed that the reduction rate of CoQ1 to $CoQ1H_2$, oxygen consumption rates and complex I activity were reduced in hyperoxia–exposed cells as compared to those for normoxia cells. On the other hand, they showed that hyperoxia exposure resulted in an increase in the reduction of DQ to DQH_2 via an increase in NQO1 protein and activity when compared to the normoxia endothelial cells.

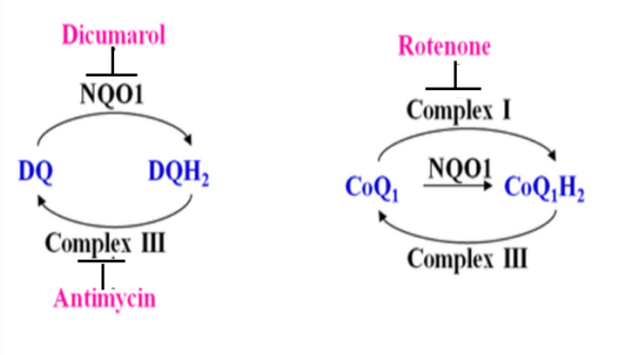

Figure 4: *Enzyme mediated reduction of quinones and their inhibitors (Gan, 2011). NQO1: NAD(P)H quinone dehydrogenase 1 is a cytosolic enzyme.*

Audi et al. assessed the disposition of DQ in isolated perfused rat lungs (Audi et al., 2003). They showed that inhibition of complex I and II reduced lung O_2 consumption by ~60%, and that this decrease was reversible with the addition of DQ to the recirculating lung perfusate.

Bongard et al. evaluated the effect of the complex I inhibitor rotenone on mitochondrial bioenergetics and respiration in cultured rat microvasculature pulmonary endothelial cells and in intact rats lungs, and assessed the efficacy of CoQ1 in reversing rotenone-induced mitochondrial dysfunction (Bongard et al., 2013) (Bongard et al.,

2015). They showed that inhibition of complex I with rotenone decreased lung ATP, increased lactate/pyruvate ratio, as an index of glycolic pathway, and increased pulmonary vascular endothelial filtration coefficient (K_f). Results in cell studies showed that complex I inhibitors affected the O_2 consumption, cell monolayer permeability and $\Delta\Psi_m$ depolarization. Furthermore, they showed that CoQ1 was able to fully reverse these rotenone-induced mitochondrial and permeability changes in intact lungs and cultured cells (Bongard et al., 2015).

Chan et al. assessed the ability of CoQ1 to reverse rotenone-induced mitochondrial dysfunction in cultured hepatocytes (Chan et al., 2002). They showed that inhibition of complex I using rotenone led to cytotoxicity, including collapse of $\Delta\Psi_m$, decrease in mitochondrial ATP production, and increase in ROS formation. The addition of CoQ1 to the cell medium reversed the cytotoxic effects of rotenone (Chan et al., 2002). As expected, inhibiting complex III with antimycin prevented CoQ1 from reversing rotenone-induced $\Delta\Psi_m$ depolarization, cytotoxicity, and cellular ATP depletion (Chan et al., 2002).

The above results suggest that the addition of DQ or CoQ1 to lung perfusate could be used to overcome the effects of hyperoxia-induced decreases in lung mitochondrial complex I and II activities on mitochondrial ETC bioenergetics/respiration.

OBJECTIVE and SPECIFIC AIMS:

The objectives of this thesis are to *1)* assess mitochondrial dysfunction in isolated perfused lungs from rats exposed to hyperoxia as a model of human ALI, and *2)* evaluate the efficacy of DQ for reversing hyperoxia-induced mitochondrial dysfunction. The overall hypothesis is that rat exposure to hyperoxia depolarizes the lung mitochondrial membrane

potential mainly due to a decrease in mitochondrial complexes I and II activities, and that this depolarization can be detected in isolated perfused lungs using R6G. Furthermore, we hypothesize that this depolarization can be reversed using DQ. We tested these hypotheses using the following specific aims.

Aim # 1: *Assess $\Delta\Psi_m$ in lungs from rats exposed to hyperoxia as a model of human ALI.* Rats will be exposed to > 95% O_2 (hyperoxia) or room air (normoxia) for 48 hours after which the lungs will be isolated and connected to a ventilation-perfusion system for measuring the disposition of R6G using the experimental-computational approach developed by Audi et. al (Audi et al., 2020). $\Delta\Psi_m$ (in mV) will be estimated from the resulting dynamic R6G venous effluent concentrations using a previously developed physiologically based pharmacokinetic (PBPK) model for pulmonary disposition of R6G developed by Audi et al (Audi et al., 2020). This time point (48 hours) was chosen since it is clinically early in the pathogenesis of hyperoxia-induced ALI.

Aim # 2: *Assess the ability of the ubiquinone analog duroquinone (DQ) to reverse hyperoxia-induced depolarization of $\Delta\Psi_m$.* For this aim, DQ will be added to the perfusate during the three phases of the experimental protocol under Aim 1 in lungs from rats exposed to > 95% O_2 (hyperoxia) or room air (normoxia) for 48 hours. $\Delta\Psi_m$ in mV will be estimated from the resulting dynamic R6G venous effluent concentrations using a PKPD model for pulmonary disposition of R6G developed by Audi et al (Audi et al., 2020).

CHAPTER 2: EXPERIMENTAL METHODS

2.1 Materials

Rhodamine-6G (R6G), verapamil hydrochloride, carbonyl cyanide 4 (trifluoromethoxy) phenylhydrazone (FCCP), duroquinone (DQ), rotenone, glutathione (GSH) and all other reagents used in experiments were purchased from Sigma-Aldrich.

2.2 Hyperoxic Exposure

Adult male Sprague Dawley rats were used for this study. For hyperoxic rats (male Sprague-Dawley rats 336.4 ± 10.15 g, n = 9), the rats were placed in a sealed Plexiglas chamber (13W x 23L x 12H inches) and exposed to >95% O_2 (hyperoxia) for 48 hours with access to food and water. The temperature inside the chamber was maintained at 20°-22°C. Their pre- and post-body weights were recorded as an index of overall health. For the normoxic lung studies, age-matched control rats (male Sprague-Dawley rats, 343.7 ± 20.04 g, n = 22) were exposed to room air (normoxia) for 48 hours. The protocol was approved by the Institutional Animal Care and Use Committees of the Zablocki Veterans Affairs Medical Center and Marquette University (Milwaukee, WI).

2.3 Isolated Perfused Rat Lung Preparation

Each rat was anesthetized with ketamine/xylazine (ketamine 80-100 mg/kg and xylazine 10mg/kg, IP), the trachea was clamped, and the chest was opened. Heparin (0.7 IU/g body wt.) was injected in the right ventricle and cannulas were placed through the pulmonary artery, the pulmonary vein via the left atrium, and the trachea. The lungs were removed and attached to a ventilation-perfusion system as shown in Figure 4. The ventilation-perfusion system is connected to pressure transducers for continuous monitoring of the airway and arterial pressure. The level of the left atrium was used as the

reference for the pulmonary arterial pressure and the venous effluent pressure was maintained at the atmospheric pressure. The lungs were perfused with Krebs-Ringer bicarbonate perfusate (control perfusate) containing (in mM) 4.7 KCl, 2.51 CaCl2, 1.19 MgSO4, 2.5 KH2PO4, 118 NaCl, 25 NaHCO3, and 5.5 glucose along with 0.5% bovine serum albumin (BSA) and 2.5% Ficoll to maintain consistent oncotic pressure (Audi et al., 2020). The lungs were ventilated at 40 breaths/min with 15% O_2, 6% CO_2, balance N_2 gas mixture with end-inspiratory and end-expiratory pressures of approximately 6 and 3 mmHg, respectively.

The control perfusate was used to prime (Masterflex roller pump) the single-pass perfusion system and ensure that the venous effluent was free of blood. The temperature was maintained at 37^{o}C and equilibrated with 15% O_2, 6% CO_2, balance N_2 resulting in perfusate PO_2, PCO_2 and pH of ~105 Torr, 40 Torr, and 7.4, respectively.

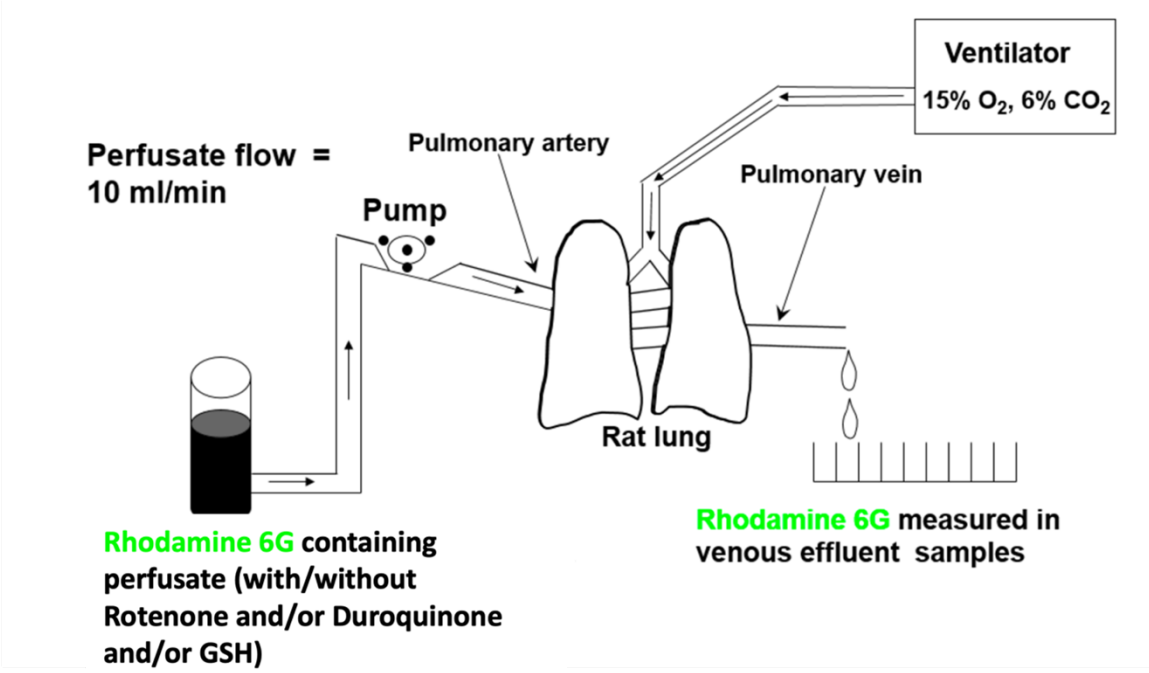

Figure 5: *Schematic diagram of ventilation-perfusion system for Isolated perfused Rat lungs (Cammarata, 2019)*

2.4 Experimental protocol to measure $\Delta\Psi_m$

The protocol to measure $\Delta\Psi_m$ in intact lungs was developed by Audi et al. (Audi et al., 2020). It consists of three phases, a loading phase where the lungs are perfused with perfusate containing R6G (0.25 μM) and the multi-drug efflux pump P-glycoprotein (Pgp) inhibitor verapamil (100 μM), a washing phase where the lungs are perfused with perfusate containing verapamil but without R6G, and an uncoupling phase where the lungs are perfused with perfusate containing the uncoupler FCCP with verapamil but no R6G. Pgp pumps R6G from the cytoplasm into the surrounding medium and therefore, verapamil inhibits the pumping of the rhodamine dye from the Pgp pump. Prior to each phase, the flow was stopped, and the reservoir emptied and then refilled with the prior perfusate. A reservoir sample was collected prior to restarting the flow. For the loading

phase, the lungs were perfused for 10 minutes (single pass) at 10 ml/min during which 2-ml venous effluent perfusate sample was collected every 40 seconds during the first 2 minutes and every minute for the remaining 8 minutes. For the washing phase, the lungs were perfused (single pass) for 5 minutes during which 2-ml venous effluent samples were collected every minute. For the uncoupling phase, the lungs were perfused (single pass) for 7 minutes during which 2-ml venous effluent samples were collected every 20 seconds for the first 2 minutes and every minute for the last 5 minutes. All the collected samples were centrifuged for 1 minute (13,000 g, 4°C) to remove any cellular components and debris. The sample supernatant was then transferred to plastic cuvettes to measure R6G emission fluorescence using the PTI system at an excitation signal of 525 nm and emission signal of 565nm (see Appendix for PTI system setup). The R6G emission signal was then converted to R6G venous effluent concentration using a standard curve as described below (Audi et al., 2020). At the end of each experiment, the lungs were weighed, dried, and reweighed to obtain the lung wet to dry weight ratio.

2.4.1 Effect of Hyperoxia on Lung R6G Uptake and Tissue $\Delta\Psi_m$

To assess $\Delta\Psi_m$ in hyperoxia-induced lungs from rats (>95% O2 for 48 hours), the above protocol was carried out in lungs from hyperoxic rats.

2.4.2 Effect of Rotenone on R6G lung Uptake and Lung $\Delta\Psi_m$

To assess the ability of the above protocol to detect $\Delta\Psi_m$ depolarization due to a decrease in complex I activity (positive control), experiments were carried out in lungs from normoxic rats for which mitochondrial complex I was inhibited by adding rotenone (complex I inhibitor, 40 μM) along with verapamil to the perfusate for all three phases.

2.4.3 Ability of DQ to Revere Rotenone-induced Changes in Lung R6G Uptake and Lung Tissue ΔΨm in Lungs from Normoxic Rats

To assess the ability of DQ to reverse $\Delta\Psi_m$ depolarization caused by inhibition of complex I, the above protocol was repeated in normoxic lungs perfused with both rotenone (40μM) and DQ (100 μM) added to the perfusate along with verapamil for all three phases.

DQ can potentially undergo a one-electron reduction to durosemiquinone on passage through the pulmonary circulation (Audi et al., 2003)(Merker et al., 2004), which in turn auto-oxidizes to generate hydrogen peroxide (H_2O_2) or disproportionate to DQH_2 and DQ (Merker et al., 2004). To counter the potential pro-oxidant effects of durosemiquinone, we repeated the protocol in a separate group of normoxic lungs (n = 7) with rotenone, glutathione (GSH, 16 μM)(Adams et al., 1983), and either DQ or its vehicle (DMSO) added to the perfusate for all three phases. The concentration of GSH used is equal to the arterial plasma GSH concentration in rats (Adams et al., 1983).

2.4.4 Ability of DQ to Reverse Hyperoxia-induced Changes in Lung R6g Uptake and lung ΔΨm depolarization

To assess the ability of DQ to reverse hyperoxia-induced $\Delta\Psi_m$ depolarization, the above protocol was repeated in hyperoxic lungs perfused DQ (100 μM) and GSH (16 μM) added to the perfusate along with verapamil for all 3 phases.

2.4.5 Effect of DQ vehicle (DMSO) on $\Delta\Psi_m$ depolarization in rotenone-induced lungs from rats

To assess the effect of DQ vehicle (DMSO) on rotenone-induced R6G pulmonary disposition and $\Delta\Psi_m$ depolarization, the above protocol was repeated in lungs perfused with perfusate containing rotenone and the DQ vehicle (DMSO). The protocol was then repeated with rotenone and DMSO add to perfusate for all three phases.

2.4.6 Data Analysis

The dynamic R6G emission fluorescent data obtained from the PTI Felix software was exported to Excel, where the data was averaged for each time sample for a period of 10 seconds and the slope from the standard curve was used to convert the R6G intensity to concentration.

2.4.7 Statistical Analysis

Statistical analysis was performed using SigmaPlot version 12.0 (Systat Software Inc., San Jose, CA). The values between two data sets were compared using unpaired *t*-test analysis. The statistical significance was set at $p < 0.05$.

2.5 Standard curve

For each experimental day, a proper standard curve was obtained and used to convert the R6G emission data from the collected lung samples to concentration (μM). Known concentrations of R6G dye (0μM, 0.03μM, 0.06μM, 0.125μM, 0.25μM and 0.5μM) were prepared. Each sample was treated the same as a lung sample, i.e., centrifuged (13,000 g, 4°C) for 1 minute and transferred to a cuvette, after which its 565 nm emission signal was measured with 525 nm excitation wavelength. The slope of the emission signal versus R6G concentration curve was estimated and used to convert the 565 nm emission signals of lung samples to concentrations. Standard curves were obtained with perfusate containing in addition to R6G and verapamil, DQ, rotenone and/or their vehicles depending on the experimental protocol.

CHAPTER 3: EXPERIMENTAL RESULTS

3.1 Rat treatments, body weights, lungs wet and dry weights, lungs wet/dry weight

Type	Treatment	Body weight (g)	Wet Weight (g)	Dry Weight (g)	Wet/dry weight ratio	Arterial pressure (Torr)
Normoxia (n=4)	Verapamil	338 ± 10	1.30 ± 0.05	0.218 ± 0.008	5.98 ± 0.24	4.5 ± 0.23
Hyperoxia (n=5)	Verapamil	329 ± 5	1.58 ± 0.06*	0.261± 0.007*	6.07 ± 0.14	4.40 ± 0.65
Normoxia (n=4)	Verapamil + Rotenone	348 ± 16	1.22 ± 0.05	0.214 ± 0.009	5.73 ± 0.05	4.38 ± 0.19
Normoxia (n=4)	Verapamil + Rotenone + DQ	351 ± 9	1.47 ± 0.12	0.237 ± 0.012	6.15 ± 0.24	5.88 ± 0.63
Normoxia (n=4)	Verapamil + Rotenone + DQ + GSH	343 ± 9	1.23 ± 0.06	0.213 ± 0.008	5.78 ± 0.08	5.63 ± 0.42
Hyperoxia (n=4)	Verapamil +DQ + GSH	329 ± 6	1.56 ± 0.09*	0.251 ± 0.007*	6.23 ± 0.16	4.38 ± 0.30
Normoxia (n=3)	Verapamil + Rotenone + DMSO	343 ± 9	1.29 ± 0.03	0.230 ± 0.006	5.62 ± 0.04	5.67 ± 0.44
Normoxia (n=3)	Verapamil + Rotenone + GSH + DMSO	329 ± 10	1.33 ± 0.04	0.230 ± 0.003	5.72 ± 0.09	5.16 ± 0.72

Table 1: *Rat treatment, body weight, lung wet and dry weight, and wet/dry weight ratio, and pulmonary artery pressure for flow rate of 10ml/min. Values are mean ± SE. * significantly different from normoxia.*

Hyperoxic rats lost ~ 2% of body weight during the 48-hr exposure period (from 336 ± 3 g to 329 ± 4 g). Table 1 shows rat body weights, lung wet and dry weights, and wet-to-dry weights along with pulmonary artery pressures for each of the experimental conditions studied. Two-tailed t-test analysis between the normoxic and hyperoxic lungs,

(without and with DQ) showed a significant difference in the wet weights (unpaired *t*-test, $p = 0.0085$ without DQ and $p = 0.047$ with DQ) and the dry weights (unpaired *t*-test, $p = 0.0067$ without DQ and $p = 0.027$ with DQ). Exposure to hyperoxia increased lung wet weight by ~22% (1.58 ± 0.14, n = 9) compared to normoxic lungs (1.3 ± 0.14, n = 22), with no effect on lung wet/dry weight ratio. These observations are consistent with previously published data and the hyperoxia-induced increase in lung wet weight being mainly due to cellular infiltration rather than edema. The addition of DQ and GSH to perfusate had no significant effect on the lung wet weight, wet/dry weight ratio, or pulmonary artery pressure of hyperoxic lungs. There was no difference in pulmonary artery pressure between normoxic and hyperoxia lungs.

Statistical analysis (unpaired *t*-test) between the normoxic lungs and rotenone-induced lungs (without DQ) indicated no significant difference in the wet weight ($p = 0.3$), dry weight ($p = 0.72$), wet/dry weight ($p = 0.3$) and the arterial pressure ($p = 0.21$).

Statistical analysis (unpaired *t*-test) performed between the normoxic lungs and rotenone-induced lungs with DQ indicated no significant difference in the wet weight ($p = 0.29$), dry weight ($p = 0.24$), wet/dry weight ($p = 0.29$) and the arterial pressure ($p = 0.06$).

Statistical analysis (unpaired *t*-test) was performed between the normoxic lungs and rotenone-induced lungs treated with DQ+GSH. Results showed no significant effect on the lung wet weight ($p = 0.37$), dry weight ($p = 0.67$) wet/dry weight ratio ($p = 0.46$), or pulmonary artery pressure ($p = 0.51$) due to the addition of GSH.

Statistical analysis (unpaired *t*-test) between the rotenone-induced group and the lungs treated with rotenone + DMSO (with and without GSH) showed no difference in

lung wet weight ($p = 0.13$ with GSH and $p = 0.33$ without GSH), lung dry weight ($p = 0.13$ with GSH and $p = 0.21$ without GSH), wet-to-dry weight ratio ($p = 0.91$ with GSH and $p = 0.14$ without GSH), or pulmonary artery pressure ($p = 0.51$with GSH and $p = 0.07$ without GSH).

3.2 R6G Standard curve from various treatments protocols

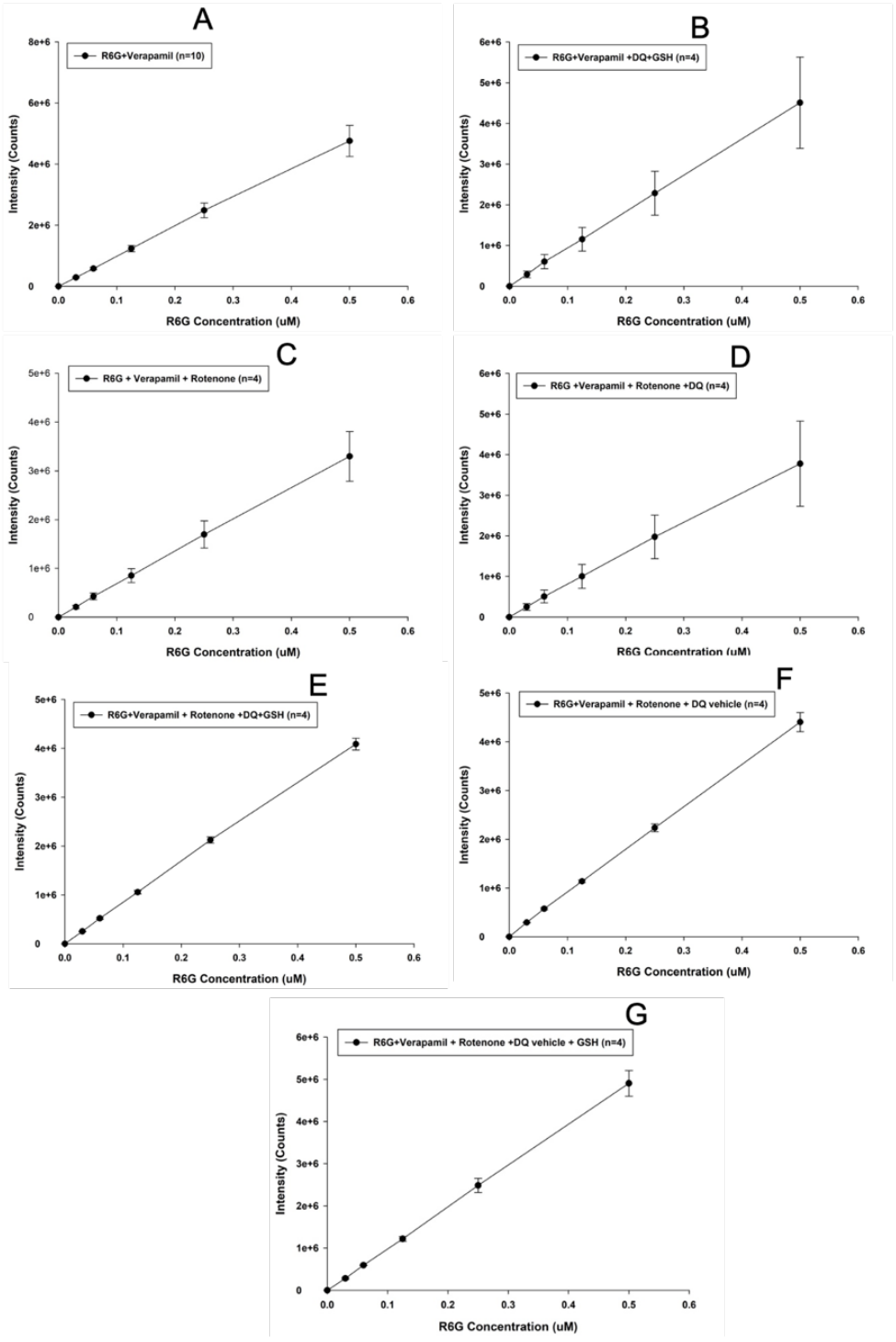

Figure 6: *Treatments standard curve (A) R6G + verapamil. (B) R6G + verapamil + DQ + GSH (C) R6G + verapamil + rotenone (D) R6G + verapamil + rotenone + DQ (E)R6G + verapamil + DQ + GSH (F) R6G + verapamil+ rotenone + DQ vehicle (DMSO) (G) R6G + verapamil+ rotenone + DQ vehicle (DMSO) + GSH.*

For a given day, a standard curve was obtained under the same experimental conditions for that day and was used to convert the R6G emission signal to R6G concentration in the recirculating perfusate. Figure 5 shows standard curves with (A) verapamil, (B) verapamil + rotenone, (C) verapamil + rotenone +DQ, (D) verapamil + rotenone + DQ + GSH, (E) verapamil + DQ + GSH (F) verapamil + rotenone + DQ vehicle (DMSO) and (G) verapamil + rotenone + GSH + DQ vehicle (DMSO) added to the standard perfusate samples.

For each of the R6G experimental protocols, the raw fluorescent intensity, in counts per second, was determined by averaging the intensity measurement values obtained for a period of 10 seconds. The sample containing only the perfusate without R6G was considered as background and the intensity value from this sample was subtracted from the intensity from all R6G concentrations. The averaged values were plotted against the known R6G concentrations. The slope was then used to convert the intensity of the R6G fluorescence to R6G concentration.

3.3 Lung uptake of R6G in normoxic and hyperoxic lungs during the three phases of the experimental protocol

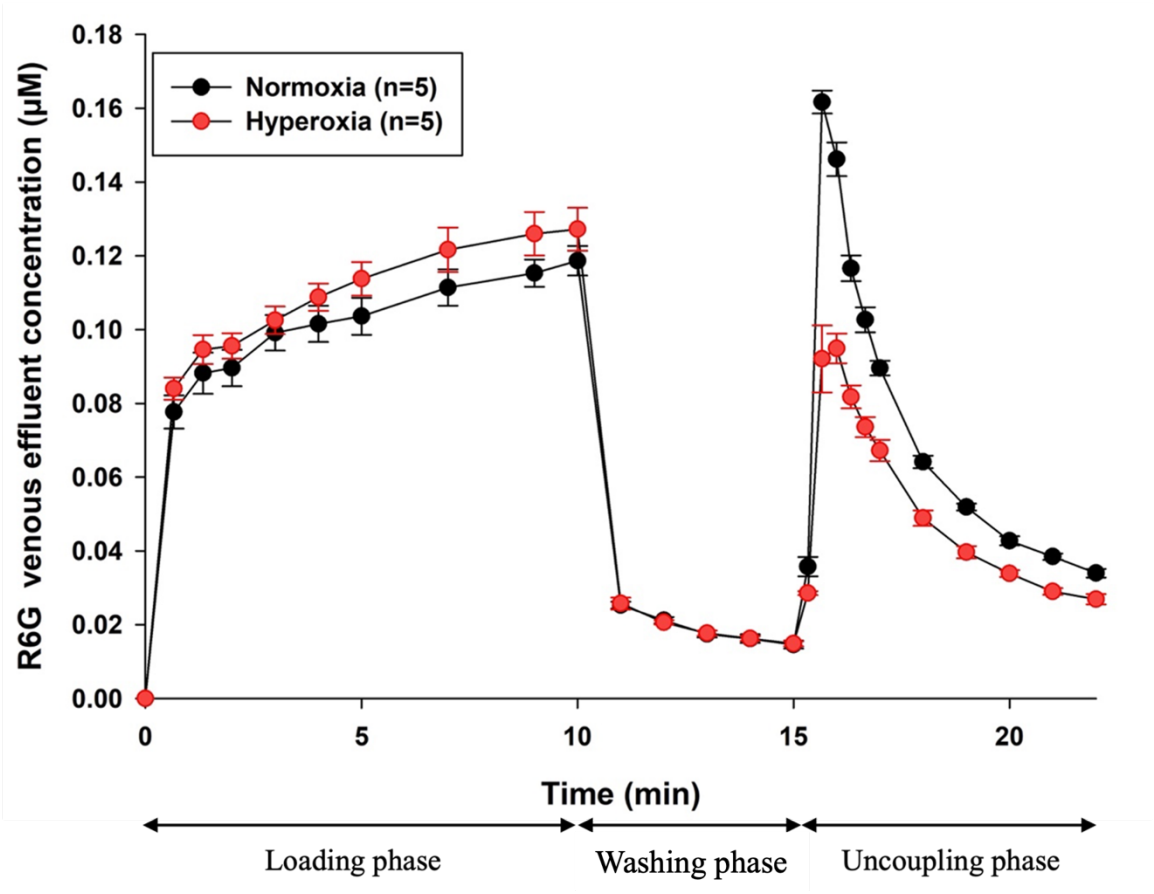

Figure 7: *Solid symbols: R6G venous effluent concentrations during the loading phase, wash phase, and uncoupling phase in normoxia (n=5) and hyperoxia(n=5). Values are mean ± SE*

Figure 7 shows the lung uptake of R6G in normoxic (n=5) and hyperoxic (n=5) lungs. For both lungs, the increase in the venous effluent R6G concentration during the uncoupling phase is consistent with the uncoupling of lung tissue mitochondria and the release of R6G that accumulated in the mitochondria during the loading phase, driven by $\Delta\psi_m$. Figure 7 shows that for hyperoxic lungs, R6G venous effluent concentrations tended to be higher during the loading phase, but significantly lower during the uncoupling phase compared to normoxic lungs. These results are consistent with less uptake of R6G by hyperoxic lungs due to partial depolarization of $\Delta\psi_m$.

3.4 Effect of mitochondrial complex I inhibitor, rotenone on R6G uptake in normoxic lungs

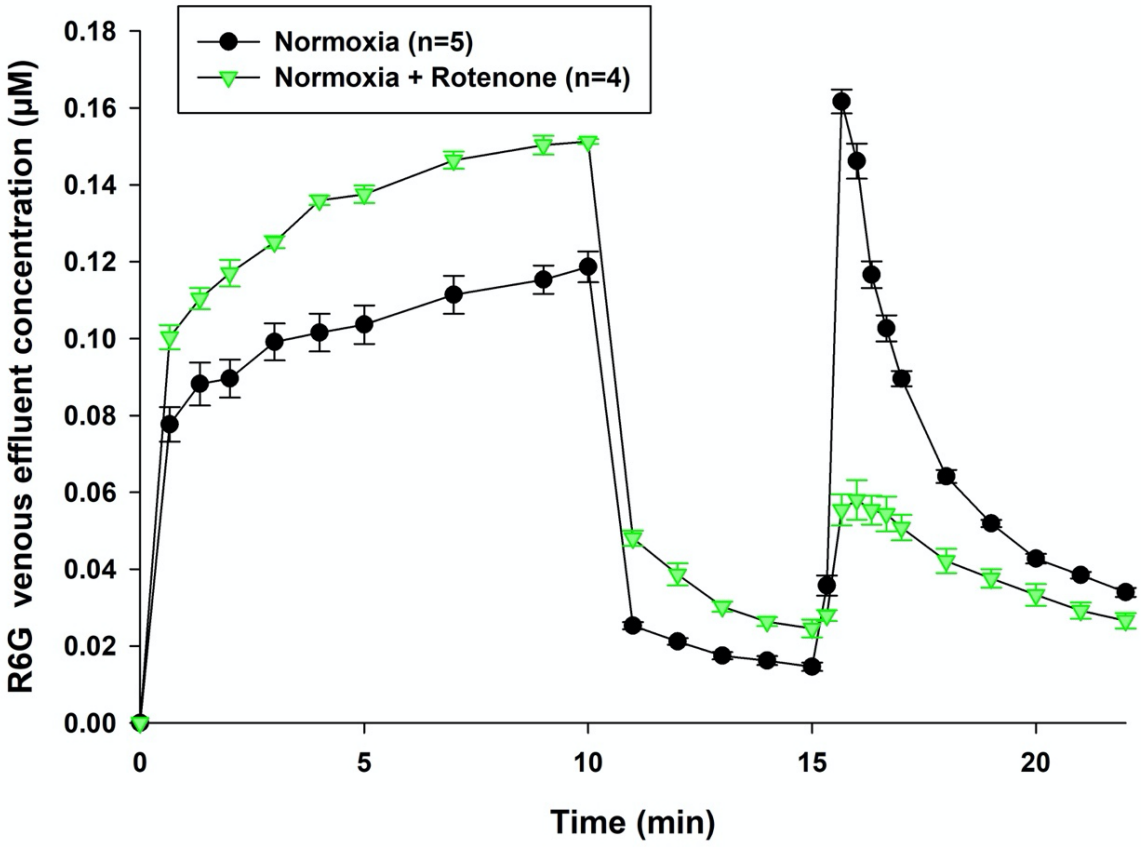

***Figure 8**: Solid symbols: R6G venous effluent concentrations during the loading phase, wash phase, and uncoupling phase in normoxia (n=5) and rotenone-treated lungs (n=5). Values are mean ± SE.*

Figure 8 shows R6G venous effluent concentration from normoxic lungs without (n=5) and with rotenone (n=4) added to the perfusate to inhibit complex I. The data shown that inhibiting complex I significantly increased R6G venous effluent concentration during the loading phase and washing phase, but significantly decreased it during the uncoupling phase. These results are consistent with a decrease in R6G lung uptake due to rotenone-induced $\Delta\psi_m$ depolarization.

3.5 Effect of DQ and its vehicle (DMSO) on R6G lung uptake in the presence of rotenone

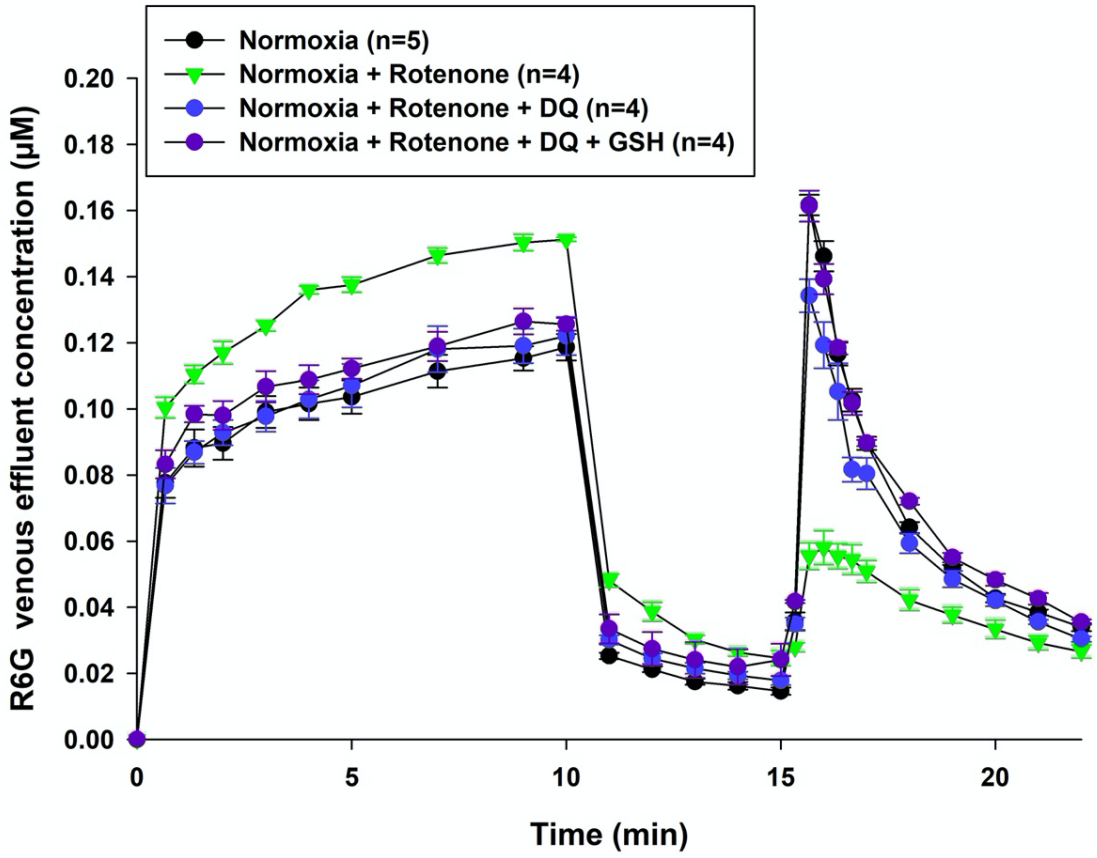

Figure 9*: Solid symbols: R6G venous effluent concentrations during the loading phase, wash phase, and uncoupling phase in normoxia (n=5), rotenone-induced lungs (n=4) and DQ treatment in rotenone induced lungs (with and without GSH, n=4). Values are mean ± SE*

.

The results in Figure 9 show that adding DQ to lung perfusate fully reversed rotenone-induced changes in R6G venous effluent concentration during all three phases. These results are consistent with the ability of lungs to reduce DQ to DQH_2 which in turn bypasses complex I and reduces cytochrome C at complex III and hence restores lung rotenone-induced $\Delta\psi_m$ depolarization.

To reduce the potential of pro-oxidant effect of adding DQ to the lung perfusate, we repeated the experiments with both DQ and GSH (16μM) added to the perfusate for all three phases. Addition of GSH (n=4) did not affect the ability of DQ to fully reverse the effects of rotenone on R6G venous effluent concentration during all three phases of the protocol.

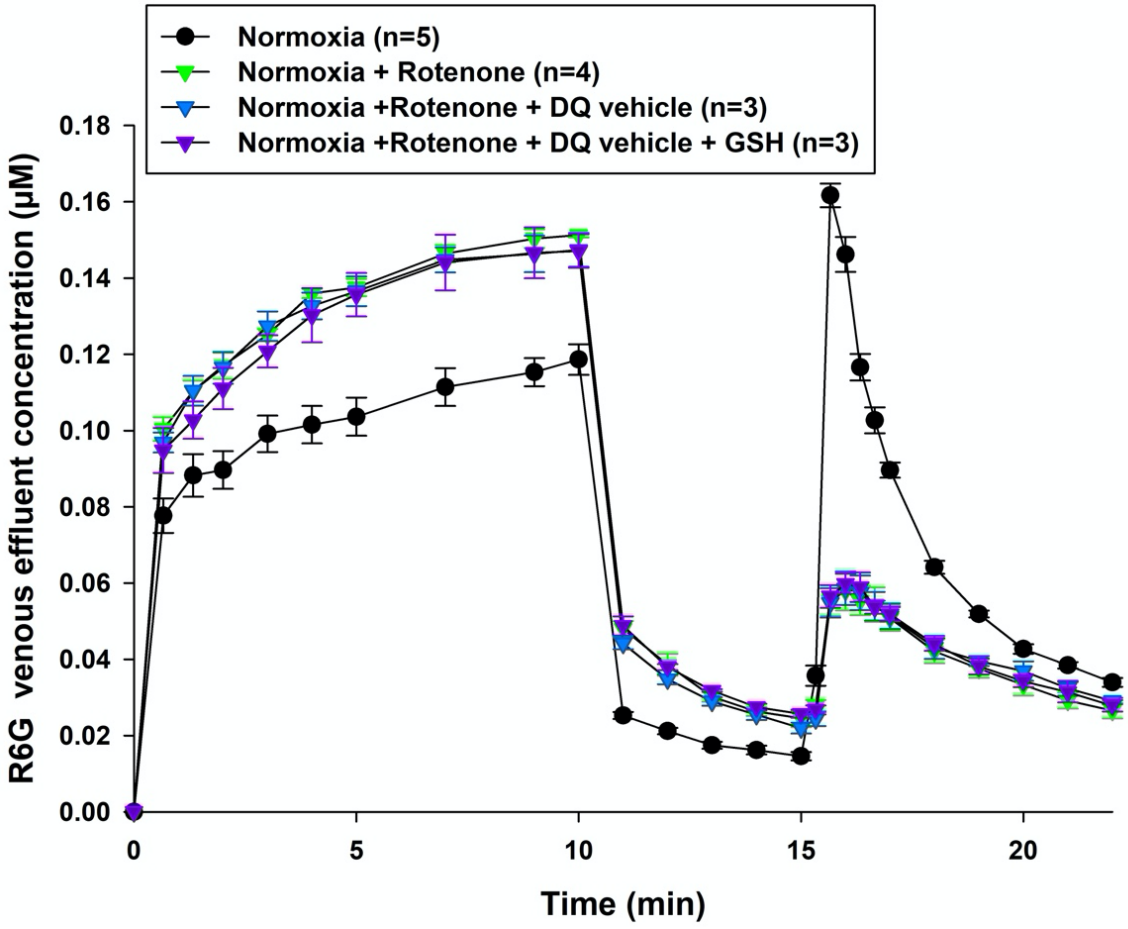

Figure 10: *Solid symbols: R6G venous effluent concentrations during the loading phase, wash phase, and uncoupling phase in normoxic lungs without (n=5) or with rotenone (n=4) and rotenone + DQ vehicle (DMSO) +GSH (n= 3), or rotenone +DMSO + GSH (n=3) added to the lung perfusate. Values are mean ± SE.*

The vehicle for rotenone and DQ is DMSO. To assess the effect of the DQ vehicle on lung R6G uptake, experiments were repeated in normoxic lungs with rotenone and DQ

vehicle (DMSO) with and without GSH (n=3 for each protocol) added to the perfusate. Figure 10 shows that DMSO, without or with GSH, had no effect on the rotenone-induced changes in R6G venous effluent concentrations during the three phases of the protocol.

3.6 Effect of Duroquinone on R6G lung uptake in hyperoxia-treated lungs from rats

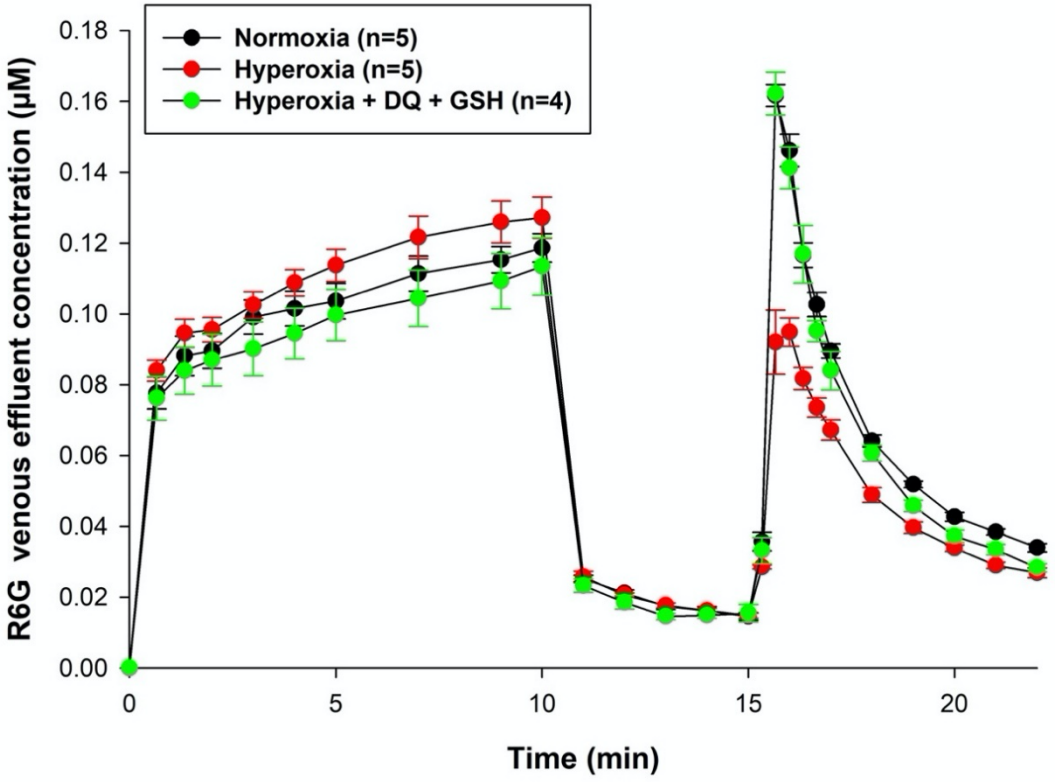

Figure 11: *Solid symbols: R6G venous effluent concentrations during the loading phase, wash phase, and uncoupling phase in normoxic lungs (n=5), hyperoxic lungs (n=5), and hyperoxic lungs with DQ added to the perfusate (n=4). Values are mean ± SE.*

To assess the efficacy of DQ to reverse hyperoxia-induced changes in R6G venous effluent concentration during the loading and uncoupling phases, we repeated the protocol in hyperoxic lungs with DQ added to the perfusate. As seen in Figure 11, addition of DQ to perfusate fully reversed hyperoxia-induced changes in R6G venous

effluent concentration during the loading and uncoupling phases consistent with the ability of DQ to overcome hyperoxia-induced decreases in complexes I and II activities by its reduction to DQH_2 which in turn bypasses complexes I and II, reduces cytochrome c at complex III and reverses hyperoxia-induced partial $\Delta\psi_m$ depolarization. Again, GSH was also added to the perfusate along with DQ to mitigate the potential pro-oxidant effects of durosemiquinone.

Chapter 4: Computational Model for Quantitative Interpretation of R6G dynamic Data and Estimation of Lung Tissue $\Delta\Psi_m$

4.1 Pharmacokinetic model for the disposition of R6G through the lungs

For quantitative interpretation of the R6G dynamic data, Audi et al. developed a physiologically based pharmacokinetic (PBPK) model for the disposition of R6G on passage through the pulmonary circulation. The model accounts for the dominant processes that determine the lung uptake of R6G on passage through the pulmonary circulation, including $\Delta\Psi_m$ (Audi et al., 2020).

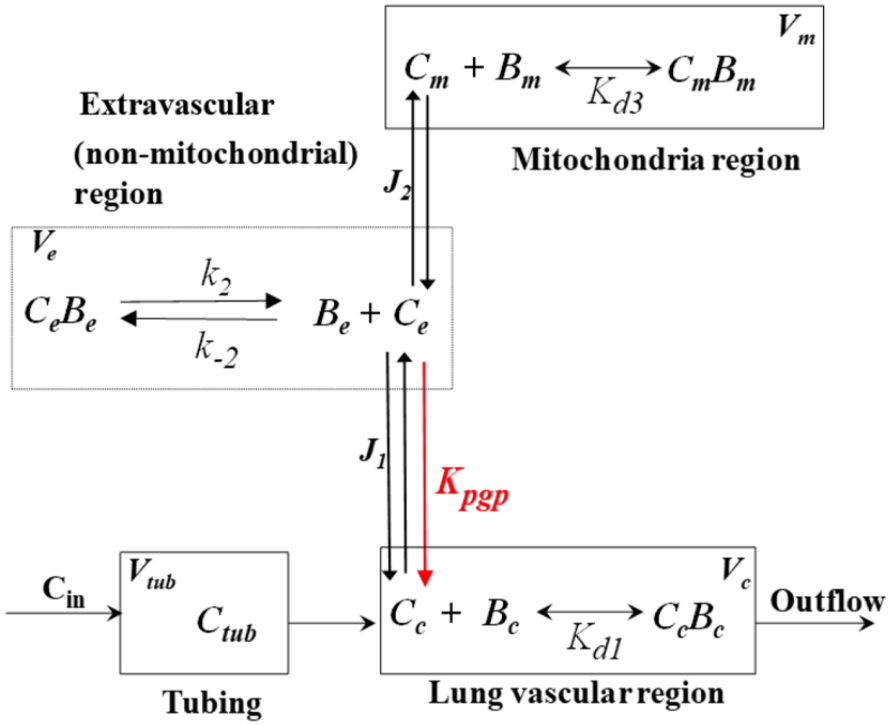

***Figure 12**:Pharmacokinetic model of the uptake and retention of R6G in the lungs (Audi et al., 2020). See glossary for definitions of the different symbols*

The model consists of four regions namely the tubing region, the lung vascular region, the extravascular region, and the mitochondrial region, with volumes (in ml) V_{tub}, V_c, V_e, and V_m, respectively. The model accounts for the dominant processes that

determine the mitochondrial uptake and retention of R6G in the lungs. K_{d1} is the dissociation equilibrium constant for the binding of R6G to BSA in the lung vascular region and is assumed to be a rapidly equilibrating process. From the vascular region, R6G passes to the extravascular region and from the extravascular region to the mitochondrial region driven by electrochemical gradients. The model uses a modified one-dimensional Goldman-Hodgkin-Katz equation to account for the R6G flux across the plasma membrane (J_1) and inner mitochondrial membrane (J_2) (Audi et al., 2020).

The model also accounts for the P-glycoprotein pump, which is a multi-drug efflux pump for the rhodamine dyes from the extravascular region to the vascular region. K_{d3} is the dissociation equilibrium constant for the binding of R6G to various proteins in the mitochondrial region and is assumed to be a rapidly equilibrating process. The differential equations that describe the rates of change of R6G concentration within each region were derived using the law of mass balance and mass action.

4.2 Derivations of model equations, model parameters

4.2.1 Glossary (Audi et al., 2020) :

[Be]	Concentration of extravascular R6G binding sites (μM)
[Bc] = [BSA]	Vascular BSA concentration (%BSA)
[Bm]	Concentration of mitochondrial R6G binding sites (μM)
[Ctub]	Free R6G concentration within the tubing region (μM)
[Ce]	Free R6G concentration within the extravascular region (μM)
[CeBe]	Concentration of bound R6G within the extravascular region (μM)
[Cc]	Free R6G concentration within the vascular region (μM)
[CcBc]	Concentration of bound R6G within the vascular region (μM)

$[\overline{C_c}]$	Total concentration of R6G within the vascular region (μM)
[Cin]	Infused R6G concentration (μM)
[Cm]	Free R6G concentration within the mitochondrial region (μM)
[CmBm]	Concentration of bound R6G within the mitochondrial region (μM)
Q	Flow rate (ml/min)
J_1	Dye flux across plasma membrane (nmol/(cm^2.min))
J_2	Dye flux across inner mitochondrial membrane (nmol/(cm^2·min))
k_1	Association rate constant of R6G - BSA binding in the vascular region (%BSA^{-1}.min^{-1})
k_{-1}	Dissociation rate constant of R6G-BSA binding within the vascular region (min^{-1})
k_2	Association rate constant of R6G – Be binding in the extravascular region (μM^{-1}.min^{-1})
k_{-2}	Dissociation rate constant of R6G – Be binding in the extravascular region (min^{-1})
k_3	Association rate constant of R6G - Bm binding in mitochondrial region (μM^{-1}.min^{-1})
k_{-3}	Dissociation rate constant of R6G - Bm binding in mitochondrial region (min^{-1})
$K_{d1} = k_{-1}/k_1$	Dissociation equilibrium constant for R6G - BSA binding in vascular region ($umol^{-1}$ x min^{-1})
$K_{d3} = k_{-3}/\bar{k}_3$	Dissociation equilibrium constant for R6G - Bm binding in the mitochondrial region

$\bar{k}_2 = k_2[B_e]$	Apparent rate constant for R6G – Be binding in the extravascular region (min^{-1})
$\bar{k}_3 = k_3[B_m]$	Apparent rate constant for R6G - Bm binding in the mitochondrial region (min^{-1})
K_{pgp}	Rate of efflux of R6G via Pgp pump from extravascular to vascular region (ml/min)
P_1	R6G permeability across plasma membrane (cm/min)
P_2	R6G permeability across mitochondrial membrane (cm/min)
S_1	Surface area of plasma membrane (cm^2)
S_2	Surface area of mitochondrial membrane (cm^2)
V_3	Apparent volume of mitochondrial region (ml)
V_{tub}	Physical volume of tubing region (ml)
V_e	Physical volume of extravascular region (ml)
V_c	Physical volume of vascular region (ml)
V_m	Physical volume of mitochondrial region = 0.02 x Ve (ml)
$\alpha = ZF/RT$	0.0374 mV^{-1} at 37ºC is a constant dependent on the universal gas constant (R), Faraday constant (F), R6G valence (Z), and absolute temperature (T)
$\Delta\Psi_m$	Mitochondrial membrane potential (mV)
$\Delta\Psi_p$	Plasma membrane potential (mV)

4.2.2 Governing model differential equations

Tubing Region

$$\frac{d[C_{tub}]}{dt} = \frac{Q}{V_{tub}}([C_{in}] - [C_{tub}]) \quad (1)$$

where [C_{in}] and [C_{tub}] are total (free + bound) concentration of R6G in reservoir and tubing regions, respectively.

Vascular region

Rates of change in the concentrations of free, [C_c], and BSA-bound, [C_cB_c], R6G within the vascular region:

$$V_c \frac{d[C_c]}{dt} = V_c(k_{-1}[C_cB_c] - k_1[C_c][B_c]) - S_1J_1 + K_{pgp}[C_e] + Q[([C_{tub}]_f - [C_c]) \quad (2)$$

The left side of the equation indicates the rate of change of free R6G concentration in the vascular region. The terms on the right side of the equation respectively account for binding and unbinding of R6G with bovine serum albumin in vascular region, R6G diffusion between vascular and extravascular regions driven by an electrochemical gradient, Pgp-mediated R6G efflux from the extravascular region back to vascular region, and R6G convective mass flux.

$$V_c \frac{d[C_cB_c]}{dt} = V_c(k_1[C_c][B_c] - k_{-1}[C_cB_c]) + Q[([C_{tub}]_b - [C_cB_c]) \quad (3)$$

where B_c = perfusate % BSA, and [C_{tub}]$_f$ and [C_{tub}]$_b$ are the free and BSA bound R6G concentrations in the tubing region such that,

$$[C_{tub}] = [C_{tub}]_f + [C_{tub}]_b \quad (4)$$

and

$$J_1 = \frac{-\alpha P_1 \Delta\Psi_p}{(e^{-\alpha\Delta\Psi_p} - 1)} \left(e^{-\alpha\Delta\Psi_p}[C_c] - [C_e]\right) \quad (5)$$

Assuming rapidly equilibrating interactions between R6G and perfusate BSA then,

$$k_1[C_cB_c] = k_1[C_c][B_c] \quad (6)$$

$$[C_cB_c] = \frac{k_1}{k_{-1}}[C_c][B_c] = \frac{[C_c][B_c]}{K_{d1}} \quad (7)$$

where K_{d1} is the R6G to BSA binding equilibrium dissociation rate constant. Let

$$[\overline{C_c}] = [C_c] + [C_cB_c] = [C_c]\left(1 + \frac{[B_c]}{K_{d1}}\right) \quad (8)$$

then addition of equations (2) and (3) after substituting equations (7) and (8) for free and bound forms of R6G in the vascular region results in:

$$V_c \frac{d[\bar{C_c}]}{dt} = -S_1 J_1 + K_{pgp}[C_e] + Q[([C_{tub}] - \overline{[C_c]}) \quad (9)$$

and

$$J_1 = \frac{-\alpha P_1 \Delta\Psi_p}{(e^{-\alpha\Delta\Psi_p - 1})} \left(e^{-\alpha\Delta\Psi_p} \frac{[\overline{C_c}]}{1+\frac{[B_c]}{K_{d1}}} - [C_e] \right) \quad (10)$$

Extravascular region

Rates of change in the concentrations of free, [C_e], and protein-bound, [C_eB_e], R6G within this region:

$$V_e \frac{d[C_e]}{dt} = V_e(k_{-2}[C_eB_e] - \overline{k_2}[C_e]) - S_2 J_2 + S_1 J_1 - K_{pgp}[C_e] \quad (11)$$

$$V_e \frac{d[C_eB_e]}{dt} = V_e - (k_{-2}[C_eB_e] + \overline{k_2}[C_e]) \quad (12)$$

where $[\overline{k_2}] = k_2[B_e]$ and

$$J_2 = \frac{-\alpha P_2 \Delta\Psi_m}{(e^{-\alpha\Delta\Psi_m - 1})} (e^{-\alpha\Delta\Psi_m}[C_e] - [C_m]) \quad (13)$$

Mitochondrial Region

Rates of change in the concentrations of free, [C_m], and protein-bound, [C_mB_m], R6G within this region:

$$V_m \frac{d[C_m]}{dt} = V_m(k_{-3}[C_mB_m] - k_3[C_m][B_m]) + S_2 J_2 \quad (14)$$

$$V_m \frac{d[C_mB_m]}{dt} = V_m(-k_{-3}[C_mB_m] + k_3[C_m][B_m]) \quad (15)$$

where [B_m] = protein concentration within mitochondrial region

Assuming rapidly equilibrating interactions between R6G and Bm then:

$$k_{-3}[C_mB_m] = k_3[C_m][B_m] \quad (16)$$

$$[C_mB_m] = \frac{[C_m]}{K_{d3}} \quad (17)$$

Where $K_{d3} = \frac{k_{-3}}{k_3[B_m]}$ is R6G and B_m binding equilibrium dissociation constant.

The addition of equations (14) and (15) after substituting equation (17) for $[C_mB_m]$ results in

$$V_m\left(1 + \frac{1}{K_{d3}}\right)\frac{d[C_m]}{dt} = V_3\frac{d[C_m]}{dt} = S_2J_2 \quad (18)$$

$where\ V_3 = V_m\left(1 + \frac{1}{K_{d3}}\right)$ is the apparent volume of the mitochondrial extravascular region.

The total R6G concentration at time *t* in the tubing and vascular region are $[C_{tub}](t)$ and $[\bar{C}_c](t)$, respectively. $[C_e](t)$ and $[C_m](t)$ refer to the free R6G concentrations in the extravascular and mitochondrial regions at time t, respectively. The bound R6G concentration at time t in the extravascular region is $[C_eB_e](t)$. The initial R6G concentration in the reservoir is $[C_{in}]$. The % BSA in the perfusate is $[B_c]$. The concentration of R6G in the binding sites in the mitochondria is $[B_m]$. The pump flow is depicted as Q (ml/min). The product of the permeability of R6G across the plasma and the mitochondrial membranes and the surface area (S) of these membranes are P_1S_1 (ml/min) and P_2S_2 (ml/min), respectively.

K_{pgp} (ml/min) represent the Pgp-mediated R6G efflux rate from extravascular to vascular region. The dissociation equilibrium constant for R6G-BSA binding in the vascular region is $K_{d1} = \frac{k_{-1}}{k_1}$. The dissociation equilibrium constant for R6G-B_m binding in the mitochondrial region is $K_{d3} = \frac{k_{-3}}{k_3[B_m]}$. The apparent volume (ml) in the mitochondrial region is $V_3 = V_m\left(1 + \frac{1}{k_{d3}}\right)$. The constant α = ZF/RT is dependent on the gas constant ®, Faraday constant (F), R6G valence (+1), and absolute temperature and is

equal to 0.0374 mV^{-1} at 37°C. The mitochondrial and plasma membrane potential are $\Delta\Psi m$ and $\Delta\Psi_p$, respectively.

The model-governing ODEs were solved numerically using the MATLAB (MathWorks) function "*ode45*", which is based on an explicit Runge-Kutta formula.

4.3 Estimation of Model parameters

Parameter	Description	Unit
$\overline{k_2}$	Apparent rate constant for R6G – Be binding in the extravascular region	(min^{-1})
k_2	Dissociation rate constant of R6G – Be binding in the extravascular region	(min^{-1})
K_{d3}	Dissociation equilibrium constant for R6G - Bm binding in the mitochondrial region	
P_1S_1	The product of the permeability of R6G across the plasma membrane and the surface area (S)	ml/min
$\Delta\Psi_m$	Mitochondrial membrane potential	mV

Table 2: *Unknow model parameters*

To reduce the number of unknown model parameters, the lung vascular volume (V_c = 0.85 ml) and the lung extravascular volume (V_e = 1.0 ml) (Audi, et al., 2003) were set to constant values. To break the correlation between V_m and $\Delta\Psi_m$, the ratio V_m/V_e was set to 0.02 (Gan et al., 2011). To break the correlation between P_1S_1 and $\Delta\Psi_p$, the value of $\Delta\Psi_p$ was set to -43mV (Gan et al., 2011). To break the correlation between K_{d1} (0.32%) and $\Delta\Psi_m$, and between P_2S_2 (1.12 ml/min) and $\Delta\Psi_m$, the values of K_{d1} and P_2S_2 were set to previously estimated values (Audi et al., 2020). Verapamil (100 μM) was assumed to completely inhibit Pgp. As such, K_{pgp} was set at 0. Thus, the unknown model parameters are $\Delta\Psi_m$, K_{d3}, $\overline{k_2}$, k_{-2} *and* P_1S_1 (Table 2).

The differential equations were solved using the MATLAB (MathWorks) function "*ode45*". The equations were solved with the following initial conditions (t = 0): $[\overline{C_c}](0) = [C_e](0) = [C_m](0) = 0$ μM and $[C_{tub}](0) = [C_{in}]$ for the loading phase, and $[C_{tub}](0) = 0$ for the washing and uncoupling phases. (Audi et al., 2020)

Chapter 5: Modeling results

5.1 Estimation of model parameters

The model solution was fit to each data set using the MATLAB function "*lsqcurvefit*", which implements a non-linear regression algorithm. The estimated values of model parameters and representative model fits to data are shown in Table 3 and Figures 12-19.

	P_1S_1 (ml/min)	$\overline{k_2}$ (ml/min)	k_{-2} (min^{-1})	K_{d3}	$\Delta\Psi_m$ (mV)
Normoxia (n=5)	46.98 ± 0.67	9.59 ± 1.79	0.113 ± 0.018	0.0136 ± 0.0008	-147.1 ± 13.2
Hyperoxia (n=5)	48.09 ± 0.80	7.43 ± 1.25	0.058 ± 0.013*	0.0094 ± 0.0004*	-109.8± 9.3*
Normoxia + Rotenone (n=4)	50.12 ± 0.88	4.66 ± 0.39*	0.065 ± 0.009	0.0056 ± 0.0005*	-57.3 ± 3.1*
Normoxia + Rotenone + DQ (n=4)	46.82 ± 0.62	9.78 ± 1.54	0.106 ± 0.012	0.0134 ± 0.0004	-131.1 ± 16.3
Normoxia + Rotenone + DQ + GSH (n=4)	47.58 ± 0.48	8.09 ± 1.34	0.127 ± 0.026	0.0135 ± 0.0012	-122.7 ± 5.7
Hyperoxia + DQ + GSH (n=4)	46.62 ± 0.73	10.62 ± 2.22	0.097 ± 0.015	0.015 ± 0.0012	-157.7± 17.2
Normoxia + Rotenone + DMSO (n=3)	50.65 ± 0.87	4.65 ± 0.58*	0.069 ± 0.007	0.0045 ± 0.0009*	-62.5 ± 4.1*
Normoxia +Rotenone + DMSO + GSH (n=3)	49.32 ± 0.79	5.69 ± 1.65	0.075 ± 0.0048	0.0064 ± 0.0017*	-60.4 ± 9.4*

Table 3: *Estimated value of model parameters. Values are mean ± SE.*different from Normoxia (t-test, $P < 0.05$).*

The values of the model parameters were estimated from fitting the mean values of various parameters in a normoxic and hyperoxic lungs. The estimated values of the model parameters (Table 3) show that rat exposure to hyperoxia depolarized lung tissue $\Delta\psi_m$ from −147 mV to −109 mV. Furthermore, exposure to hyperoxia decreased the values of K_{d3} (29%) and k_{-2} (48%) but had no significant effect on the values of $\bar{k}_2$ and

P_1S_1. As expected, inhibition of complex I activity with rotenone depolarized $\Delta\psi_m$ from −147 mV to −57 mV. Furthermore, rotenone decreased the values of $\bar{k}_2$ (50%), k_{-2} (40%), and K_{d3} (60%) compared to values in the absence of rotenone. Lung perfusion with DQ or DQ + GSH fully reversed the rotenone effect on the values of $\Delta\psi_m$ and other model parameters. The results suggest that GSH does not influence the pulmonary disposition of R6G or the ability of DQ to reverse rotenone-induced $\Delta\psi_m$ depolarization. Additional results show that adding DMSO (DQ vehicle) to the perfusate along with rotenone had no significant effect on the estimated values of the model parameters. The modeling results also show that the addition of DQ + GSH to the recirculating perfusate fully reversed hyperoxia-induced depolarization of $\Delta\psi_m$ and the effect of hyperoxia on the values of K_{d3} and k_{-2}.

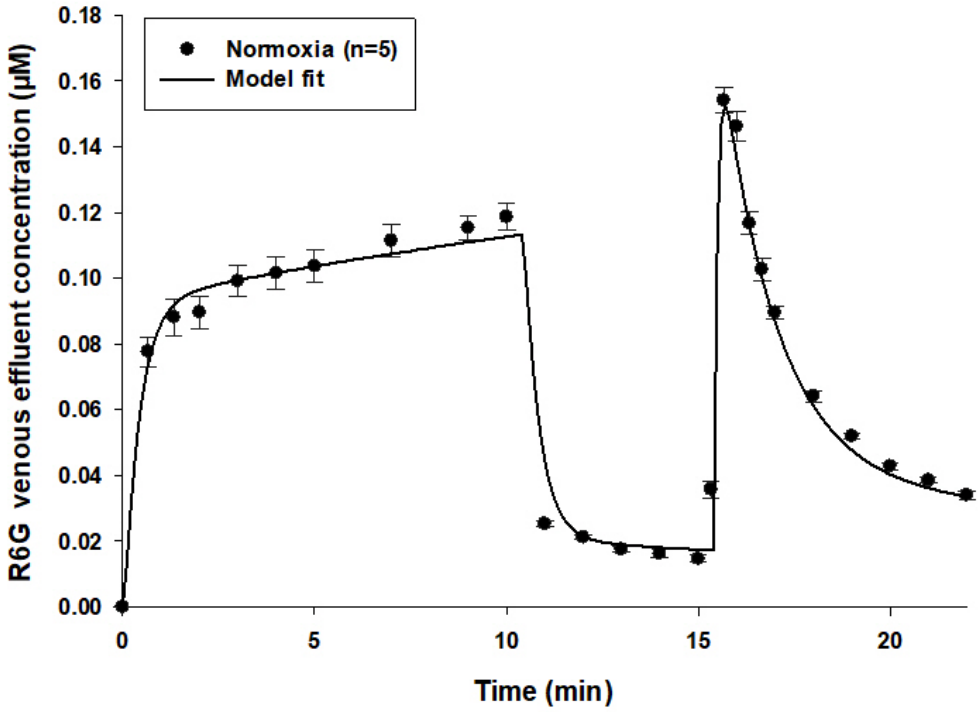

Figure 13: *Solid symbols: Normoxia R6G venous effluent concentrations (mean ± SE) during loading, washing and uncoupling phases. Solid line is model fit to data.*

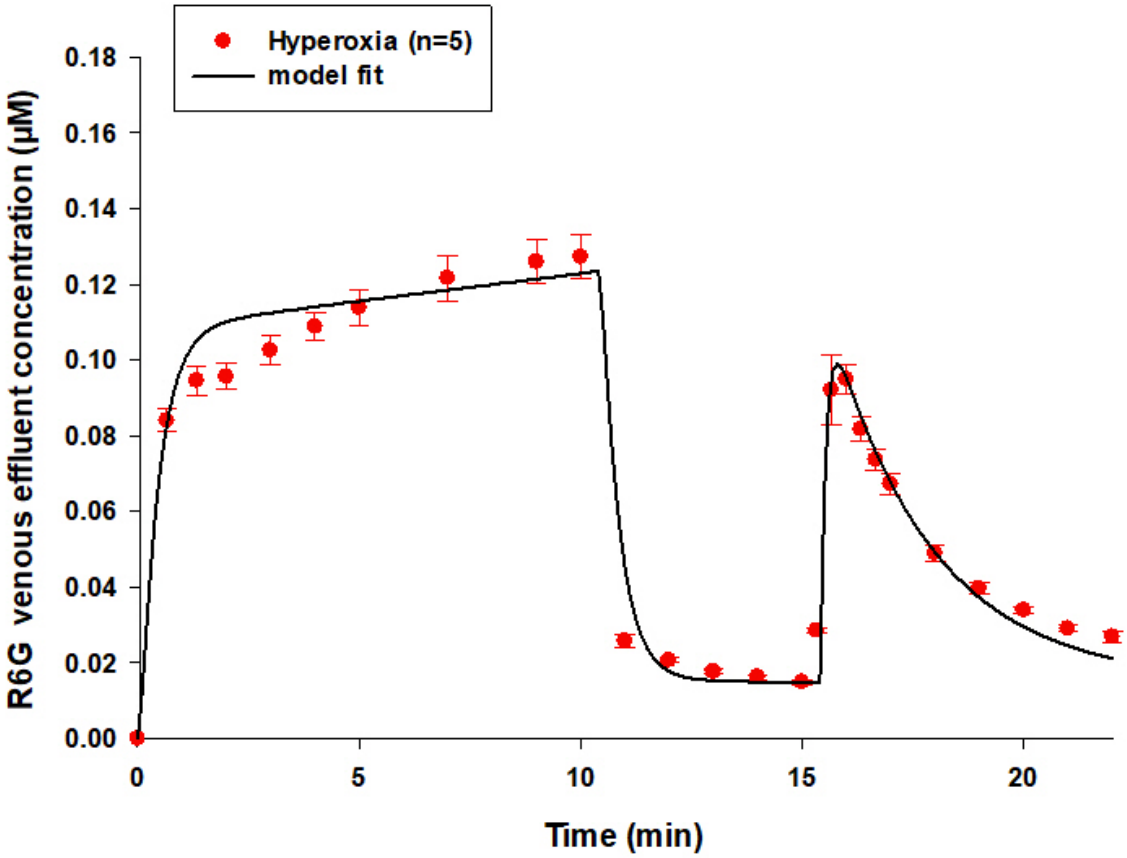

***Figure 14**: Solid symbols: Hyperoxia R6G venous effluent concentrations (mean ± SE) during loading, washing and uncoupling phases. Solid line is model fit to data.*

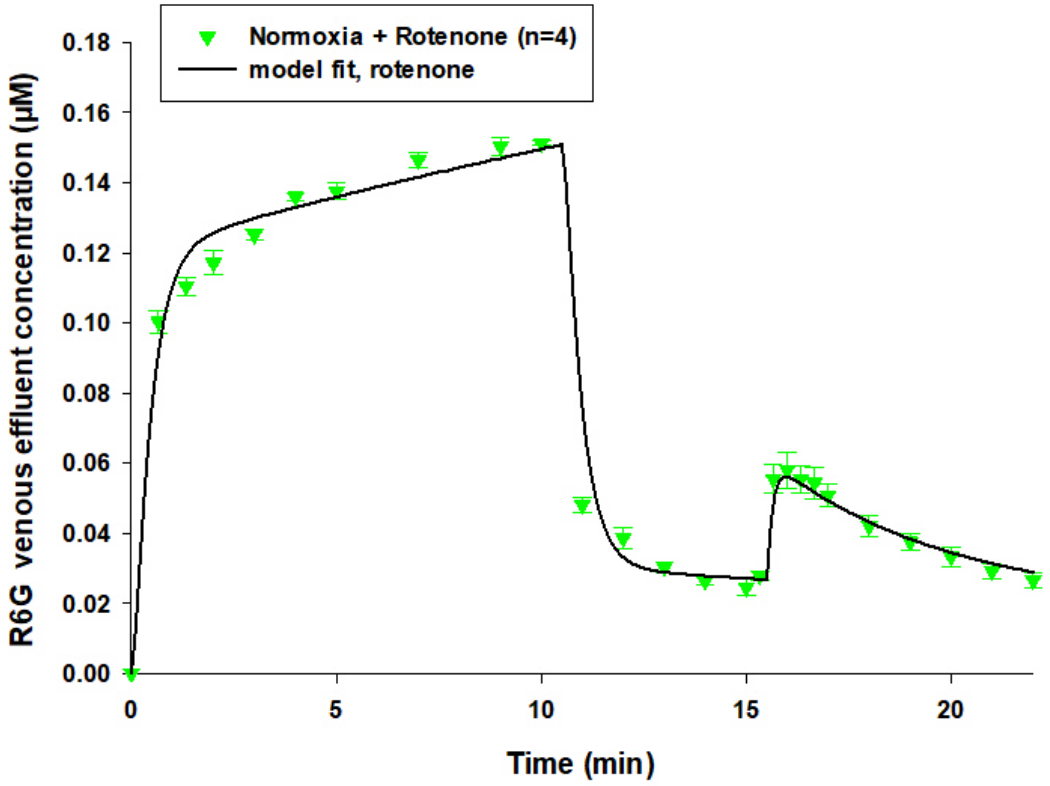

Figure 15: *Solid symbols: Rotenone-induced R6G venous effluent concentrations (mean ± SE) during loading, washing and uncoupling phases. Solid line is model fit to data.*

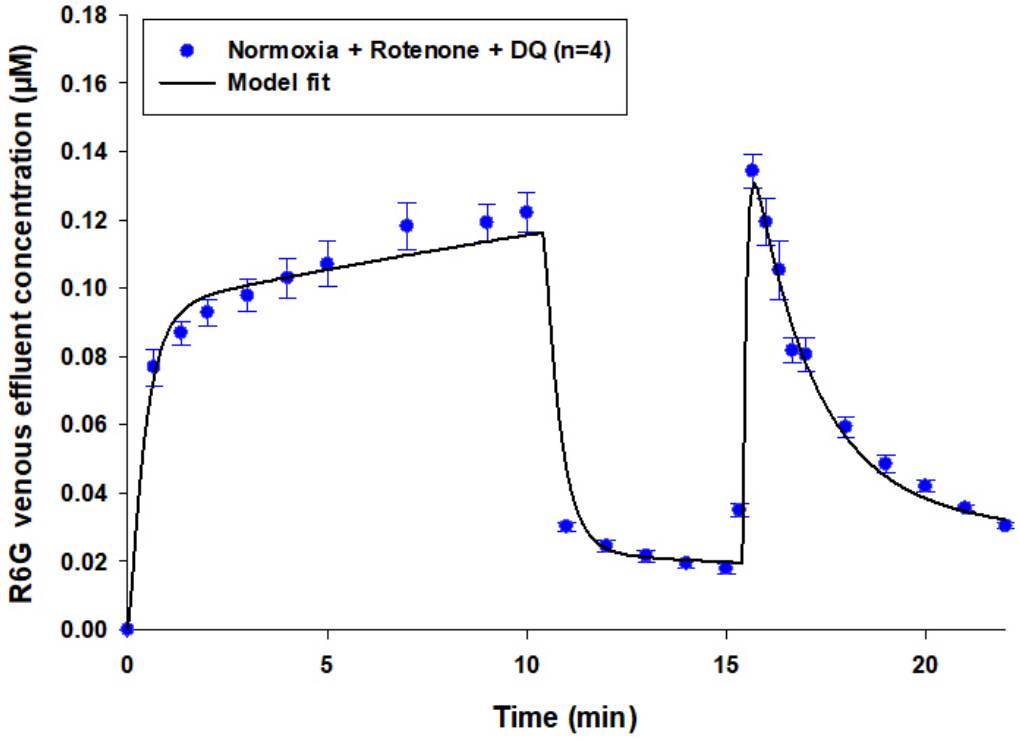

Figure 16: *Solid symbols: Rotenone +DQ R6G venous effluent concentrations (mean ± SE) during loading, washing and uncoupling phases. Solid line is model fit to data.*

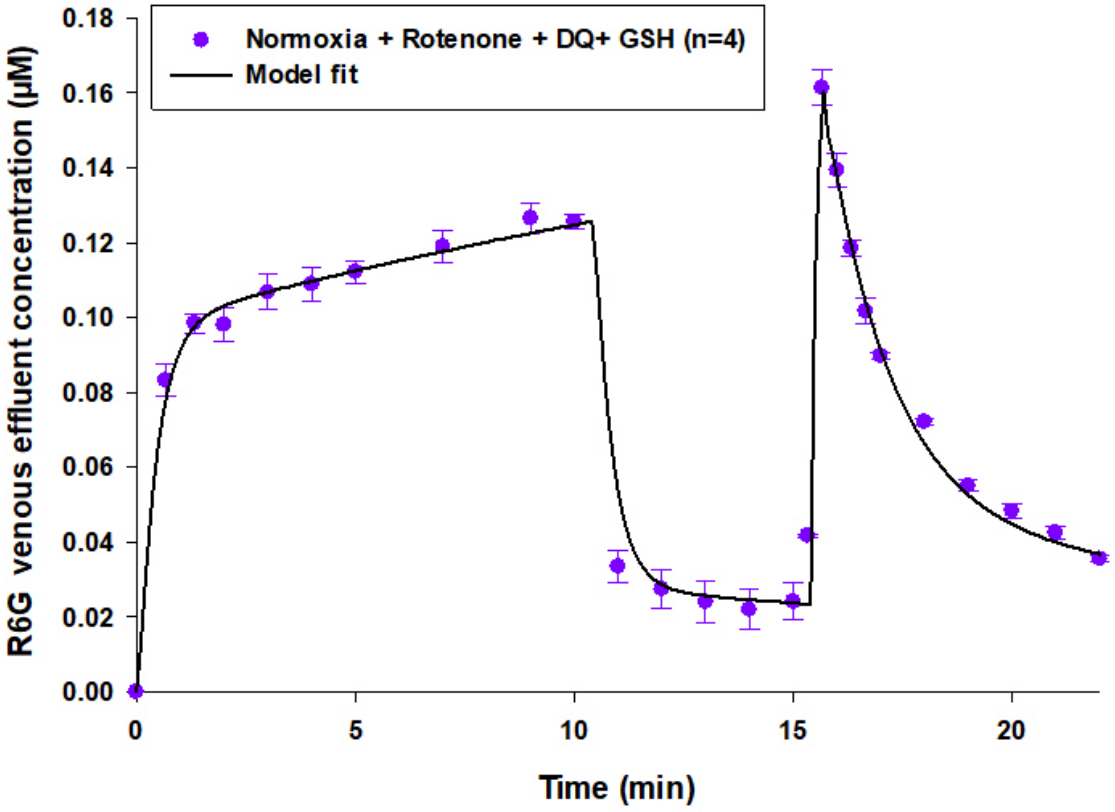

Figure 17: *Solid symbols: Rotenone +DQ+GSH R6G venous effluent concentrations (mean ± SE) during loading, washing and uncoupling phases. Solid line is model fit to data.*

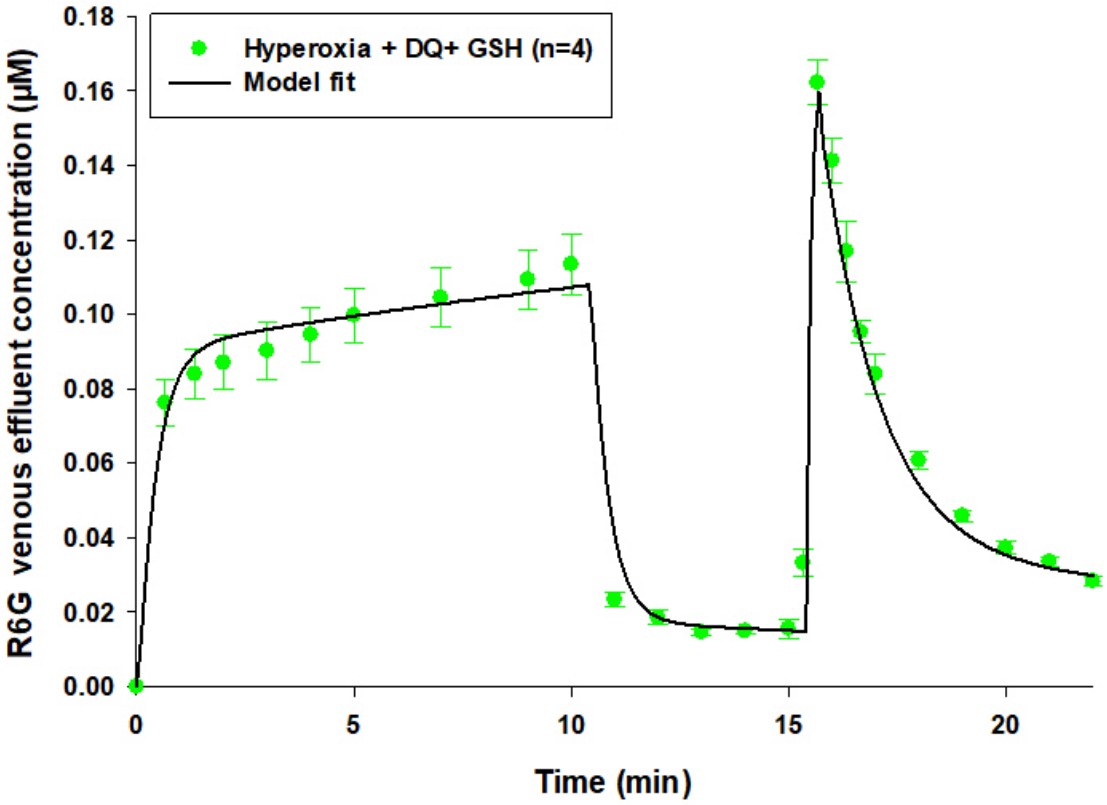

Figure 18: *Solid symbols: Hyperoxia + DQ+ GSH R6G venous effluent concentrations (mean ± SE) during loading, washing and uncoupling phases. Solid line is model fit to data.*

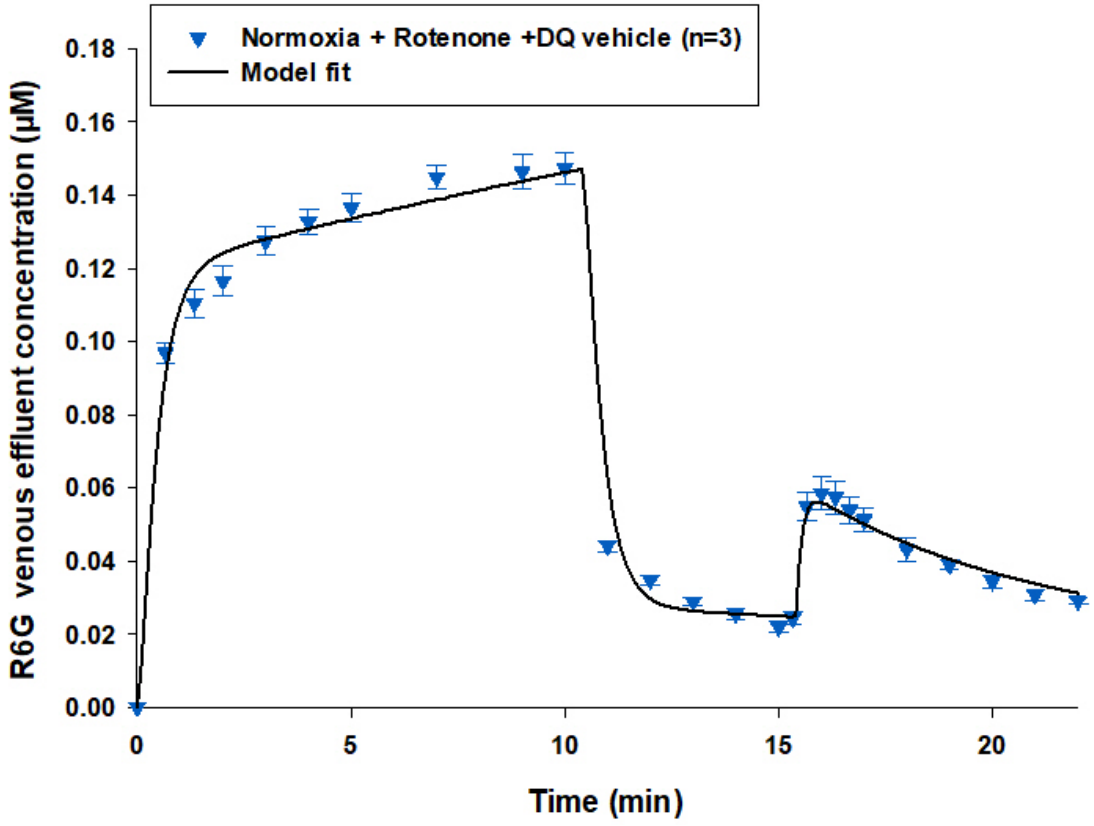

Figure 19: *Solid symbols: Rotenone + DQ vehicle(DMSO) R6G venous effluent concentrations (mean ± SE) during loading, washing and uncoupling phases. Solid line is model fit to data*

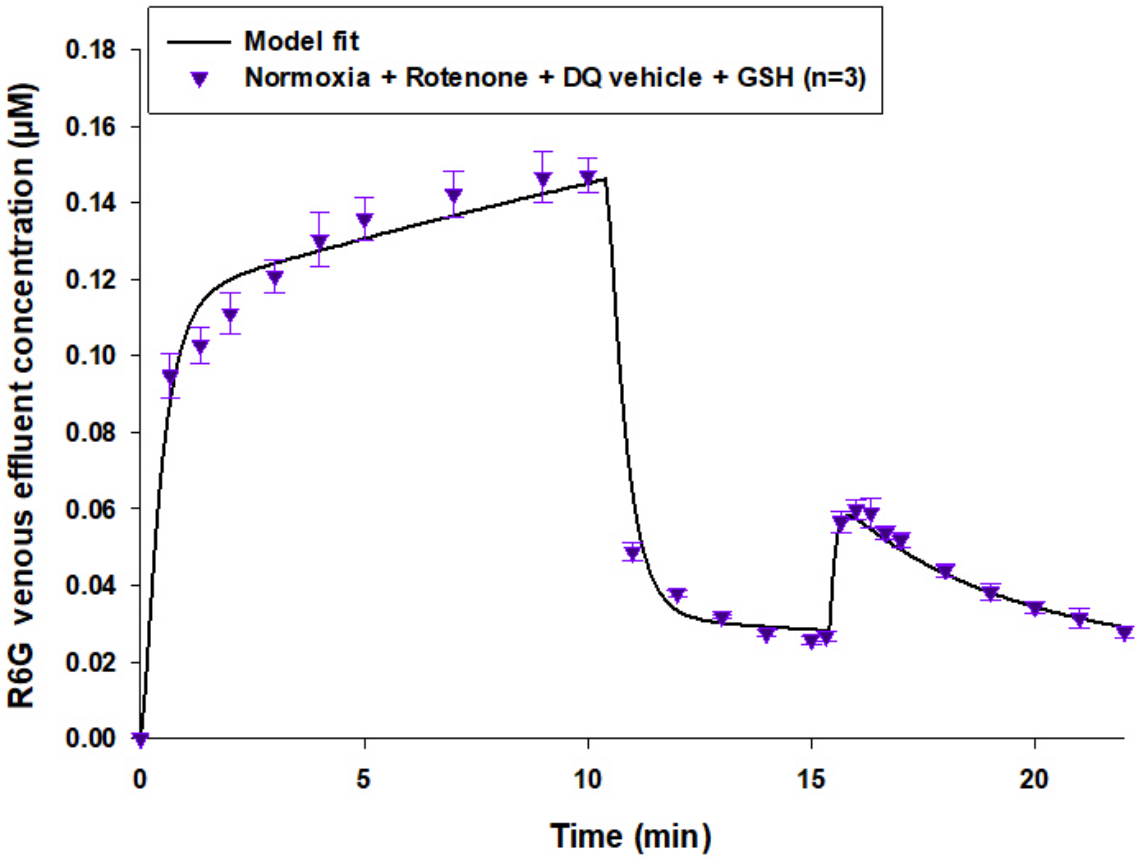

Figure 20: *Solid symbols: Rotenone + DQ vehicle (DMSO)+GSH R6G venous effluent concentrations (mean ± SE) during loading, washing and uncoupling phases. Solid line is model fit to data.*

5.2 Correlation matrix

Table 4 shows measures of precision and estimability of model parameters, including 95% confidence interval and correlation matrix.

The correlation matrix provides a measure of interdependence between a given parameter and each of the others. For the correlation matrix, the ij^{th} entry of the correlation matrix is the correlation coefficient between the i^{th} and j^{th} model parameters. The values closer to 0 indicate that the parameters are not correlated, and the values closer to 1 and -1 indicate that the parameters are correlated.

Table 4 shows that for R6G dynamic data from both normoxic and hyperoxic lungs, the correlation coefficients between model parameters are also relatively small. A correlation coefficient of 1 means that for a change in one variable can be completely compensate for by a change in another parameter. As such, the two parameters are completely dependent and cannot be independently identified or estimated.

For a given parameter, the 95% confidence interval represents the range of values for the model parameter that provide a similar fit of the model to data. The wider the 95% confidence interval, the less confidence you have in the estimated value of the model parameter.

The correlation coefficients and 95% confidence intervals were estimated using the following equation.

Correlation Coefficient: For a model with P parameters, the correlation matrix, CC, is a P x P matrix obtained as follows:

$$CC_{ij} = \frac{\left(X^T X\right)^{-1}_{ij}}{\sqrt{\left(X^T X\right)^{-1}_{ii}\left(X^T X\right)^{-1}_{jj}}}\ , i = 1, \ldots, P \text{ and } j = 1, \ldots, P$$

where X is the Jacobian matrix. It is an N x P matrix, where N is the number of data points. In the above equation, $CC_{ij} = CC_{ji}$ = correlation coefficient between the ith and jth parameters ($i \neq j$).

Confidence Interval: For a model with N parameters, the 100 (1– α) % asymptotic confidence intervals, i.e. 100(1– α) % chance that the interval contains the true value of the model parameter that best fit model to data, can be estimated using the following equation.

$$\beta_j \pm Se\left(\beta_j\right) t\left(N - P; \frac{\alpha}{2}\right)$$

where β_j is the value of the jth model parameter that best fit model to data, N is the number of data points, $t\left(N - P; \frac{\alpha}{2}\right)$ is the upper $\alpha/2$ quantile for student t-distribution with N – P degrees of freedom, and $S_e(\beta_j)$ is the standard error of the jth parameter β_j.

$$Se\left(\beta_j\right) = s\sqrt{\left\{\left(X^T X\right)^{-1}\right\}_{ii}}$$

where X is the Jacobian matrix and $\left\{\left(X^T X\right)^{-1}\right\}_{jj}$ is equal to the jth diagonal element of the matrix $\left(X^T X\right)^{-1}$ and s^2 = SSD/(N-P) where SSD is the sum of square difference between data and best model fit to data.

	Estimated Model Parameters	Measure of Precision of Model Parameter Estimates					
		95% confidence interval	Correlation Matrix				
Normoxic mean R6G data							
			$\overline{k_2}$	k_{-2}	K_{d3}	$\Delta\Psi_m$	P_1S_1
$\overline{k_2}$	9.54	± 1.67	1				
k_{-2}	0.13	± 0.02	0.66	1			
K_{d3}	0.0133	± 0.0008	0.43	0.12	1		
$\Delta\Psi_m$	-142.95	± 13.32	0.37	0.44	0.73	1	
P_1S_1	46.95	± 0.82	0.77	0.29	0.43	0.18	1
Hyperoxic mean R6G data							
			$\overline{k_2}$	k_{-2}	K_{d3}	$\Delta\Psi_m$	P_1S_1
$\overline{k_2}$	7.85	± 1.53	1				
k_2	0.074	± 0.014	0.80	1			
K_{d3}	0.0092	± 0.0005	0.56	0.30	1		
$\Delta\Psi_m$	-111.43	± 10.88	-0.19	0.09	0.25	1	
P_1S_1	49.83	± 2.22	-0.87	-0.58	-0.59	0.31	1

Table 4: *Estimates of model parameters from normoxic and hyperoxic mean R6G data and measures of precision of these estimates, namely 95% confidence intervals and the correlation matrix.*

Chapter 6: Discussion, Conclusions & Future Direction

One objective of this thesis was to use a previously developed experimental and computational approach to assess the effect of rat exposure to hyperoxia on lung tissue $\Delta\Psi_m$ in intact perfused lungs using the lipophilic cationic dye, R6G. The results show that rat exposure to hyperoxia (>95% O_2 for 48 hours) resulted in a partial depolarization (– 33 mV) of lung $\Delta\psi_m$. The ability of the experimental-computational approach for detecting $\Delta\psi_m$ depolarization in isolated perfused rat lungs was assessed in normoxic lungs perfused with the complex I inhibitor, rotenone, which depolarized lung tissue $\Delta\psi_m$ from – 147 mV to – 57 mV, a –90 mV depolarization. Another objective was to assess the ability of duroquinone (DQ) in reversing lung tissue $\Delta\psi_m$ depolarization resulting from decreases in the activities of mitochondrial complexes I and II. The results show that DQ was able to fully reverse both rotenone-induced and hyperoxia-induced partial depolarization of lung tissue $\Delta\psi_m$. On passages through lungs, DQ is reduced to DQH_2, which in turn bypasses complexes I and II and reduces cytochrome c at complex III and in the process reverse any depolarization in $\Delta\psi_m$ resulting from a decrease in complex I activities. To our knowledge, this is the first report of measuring the ΔΨm depolarization in hyperoxia-induced ALI in intact lungs from rats.

The normal range for $\Delta\Psi_m$ in lungs and cultured pulmonary endothelial cells is between -136 to -150 mV (Gan et al., 2011)(Audi et al., 2020) (Bagkos et al., 2014)(Alpert et al., 2018). A lower or depolarized value is indicative of mitochondrial dysfunction(Bhandari et al., 2013). Rat exposure to hyperoxia induces mitochondrial changes, including decreased lung tissue activities of mitochondrial complexes I and II

(Sepehr et al., 2013), which in turns causes partial depolarization of lung $\Delta\Psi_m$. Functional implications of the measured hyperoxia-induced partial depolarization of $\Delta\Psi_m$ in the present study could lower mitochondrial ATP production rate. This is consistent with results from Audi et al. showing that $\Delta\psi_m$ recovery from ADP-induced depolarization (state 3) in mitochondria isolated from hyperoxic lungs was substantially slower than that from normoxic lungs (Audi et al., 2017). Fisher AB reported that rat exposure to 100% O_2 for 48 hours increased lung lactate production rate (78%) and lactate to pyruvate ratio (105%) as an index of glycolytic ATP production. Fisher AB also reported an increase in the glycolytic ATP production and the lactate to pyruvate ratio and concluded that this increase in glycolytic ATP production could compensate for a decrease in ATP production via mitochondrial oxidative phosphorylation (Fisher & Beers, 2008). Bassett et al reported an increase in the rate of glucose utilization and an increase in the rate of lactate + pyruvate production by ~99% in lungs of rats when exposed to hyperoxia (100% O_2 for just 24 hours), consistent with the need of cells to increase glycolytic ATP production to compensate for decreased ATP production via mitochondrial oxidative phosphorylation, potentially due to hyperoxia-induced partial depolarization of lung tissue $\Delta\psi_m$.(Bassett et al., 1992) These results suggest potentially significant functional implications for the hyperoxia-induced partial depolarization of lung tissue $\Delta\psi m$ measured in the present study.

Previous studies have evaluated the impact of inhibiting mitochondrial complex I and/or II on mitochondrial bioenergetics and respiration in intact lungs and cultured endothelial cells, and have assessed the ability of exogenous quinone compounds such as DQ and CoQ1 to restore the lung/cell bioenergetics and respiration (Audi et al., 2003)

(Bongard et al., 2013) (Bongard et al., 2015). Audi et al reported that the inhibition of complex I and II decreased the oxygen consumption by ~60% and that this decrease was fully reversed by the addition of DQ to the recirculating perfusate (Audi et al., 2003). These data are consistent with the ability of DQH_2 to bypass complexes I and II and reduce cytochrome c at complex III. Bongard et al. reported that inhibition of complex I decreased the ATP levels by ~ 60% , and increased lactate/pyruvate ratio by ~ 200%, as an index of the glycolic pathway and reported that these changes were fully reversed in the presence of CoQ_1 (Bongard et al., 2013). Bongard et al. also assessed the effects of rotenone on ATP level and $\Delta\psi_m$ in rat pulmonary microvascular endothelial cells in culture, and on the ability of CoQ_1 to reverse those effects (Bongard et al., 2015). They showed that rotenone decreased ATP by 75%, depolarized $\Delta\psi_m$ from –129 mV to –93 mV, decreased O_2 consumption by 85%, and increased cell monolayer permeability and reported that these effects were completely reversed when COQ1 was present along with the inhibitor (Bongard et al., 2015). The effect of rotenone on cellular $\Delta\psi_m$ in these previous studies is consistent with the results in the present study in intact functioning lungs.

DQ can be reduced to DQH_2 as well as durosemiquinone, which auto-oxidize back to DQ with superoxide as a by-product, which in turn dismutates to form H_2O_2, or disproportionate to DQH_2 and DQ (Merker et al., 2004)(Audi et al., 2003). Audi et al. showed that the reduction of DQ is predominantly via NQO1, which is a two-electron reduction, on passage through the rat and mouse pulmonary circulations (Audi et al., 2003). For the present study, to counter any potential pro-oxidant effect due to durosemiquinone, GSH was added along with DQ to the lung perfusate.

DQH_2 can serve as an anti-oxidant by reducing H_2O_2 to H_2O in addition to reducing complex III (Merker et al., 2004). The addition of GSH alone to the perfusate did not have an effect on the rotenone-induced $\Delta\psi_m$ depolarization (Figure 9) which suggests that the ability of DQ to fully reverse rotenone-induced $\Delta\psi_m$ depolarization is not due to the anti-oxidant effect of DQH_2, but rather due to the ability of DQH_2 to bypass complexes I and II and reduce cytochrome c at complex III.

Coenzyme Q10 (CoQ_{10}) is a ubiquinone analog and is widely available over the counter as a dietary supplement and recommended by primary care providers and specialists alike (Sood et al., 2021). Previous studies have assessed the effect of CoQ_{10} on sepsis-induced acute lung injury (Li et al., 2019). The results showed that CoQ_{10} increased the survival rate and alleviated pulmonary edema in rats with sepsis-induced ALI. The ability of CoQ_{10} to demonstrate some beneficial effect in the treatment of mitochondrial disease is thought to rely mainly on its ability to restore electron flow in the mitochondrial respiratory chain and replenish cellular antioxidant capacity (Neergheen et al., 2017). CoQ_{10} in patients with mitochondrial disorders have shown to have an impact on the aerobic capacity in lungs (Sood et al., 2021).

The computational model provides a framework for mechanistic interpretation of the data and for estimation of the values of parameters descriptive of the dominant processes determining the R6G uptake by the lung tissue and mitochondria, including the $\Delta\Psi_m$. For the computational analysis of the R6G data using the PBPK model, the values of lung vascular volume ($V_c = 0.85$) and lung extravascular volume ($V_e = 1$) were fixed to values estimated form normal rats, and hence were assumed to be unaffected by exposure to hyperoxia. Crapo et al. showed that rat exposure to 100% O_2 for 40 hours had no

significant effect on lung vascular volume (Crapo et al., 1980). Another study by Block and Fisher also showed that hyperoxia exposure (100% O_2 for 48 hours) did not affect the lung vascular flow distribution (Block & Fisher, 1977). Moreover, simulations using the PBPK model predict that a 15% decrease in vascular volume would result in only a –2 mV change in the estimated value of $\Delta\psi_m$.

One of the questions that arises is the effect of hyperoxia on the plasma membrane potential. For the present study, the value of $\Delta\Psi_p$ was fixed to a previously estimated value (-43mV) and was assumed to be unaffected by exposure to hyperoxia (Gan et al., 2011). However, $\Delta\Psi_p$ could be altered by injury or disease, and model simulations show that depolarization of $\Delta\Psi_p$ could alias for $\Delta\psi_m$ depolarization as far as changes in dynamic R6G data. However, not much is known about the effect of exposure to hyperoxia on $\Delta\Psi_p$. Changes in $\Delta\Psi_p$ due to hyperoxia could be measured using fluorescent dyes sensitive to $\Delta\Psi_p$ such as the anionic probe bis-oxonol (Landry et eal., 1991) (al-Mehdi et al., 1997)(Zhang et al., 2005), but such experiments are outside the scope of the present study. The fact that the addition of DQ to the lung perfusate fully reversed hyperoxia-induced changes in the R6G concentration data (Figure 10) and in the estimated values of the model parameters (Table 3), including $\Delta\psi_m$, suggests that the assumption of no difference in the values of $\Delta\psi_p$ (and vascular volume) between normoxic and hyperoxic lungs is reasonable.

Previous studies have shown that complex I and complex II activity decreases when exposed to hyperoxia (Sepehr et al., 2013). However, the results from the present study do not provide information about the individual contributions of hyperoxia-induced decreases in complex I versus complex II activity to the measured partial depolarization

of $\Delta\psi_m$. In the electron transport chain, mitochondrial membrane potential is generated by pumping electrons from the mitochondrial matrix into the intermembrane space at complexes I, III and IV. Normally, 10 H^+ are pumped via the complex I-III-IV versus 6 H^+ via the complex II-III-IV pathway. Based on this, a decrease in complex I would be expected to have a higher impact on $\Delta\psi_m$ than a decrease in complex II activity. However, studies by Audi et al. reported that 48% decrease in mitochondrial complex I activity when exposed to hyperoxia (85% for 48 hours) compared to normoxic lungs did not produce a detectable change in whole lung O_2 consumption rate (Audi et al., 2008). One possible explanation for this result is that the complex I activity is normally in excess compared with the rate of electron flow through the respiratory chain. This is consistent with the results of a study by Barrientos and Moraes, in which the effects of complex I impairment on cell respiration were evaluated in a rotenone-treated human osteosarcoma-derived cell line (Barrientos et al., 1999). They showed that complex I activity was inhibited by as much as 35%, with little effect (5%) on cell respiration. Another possible explanation could be due to the compensatory mechanism of cells to sustain cell respiration in complex I impaired hyperoxia-induced lungs.

Rotenone and hyperoxia decreased the values of the model parameters descriptive of R6G binding ($\bar{k}_2$, k_{-2}, and K_{d3}) within the non-mitochondrial and mitochondrial regions. This could be due to the effect of rotenone or hyperoxia on the number of R6G binding sites within the non-mitochondrial and mitochondrial regions and/or on the R6G binding kinetics due to changes in the redox states within these regions resulting from the partial depolarization of $\Delta\psi_m$ (Dell'Antone et al., 1972). The fact that the addition of DQ to perfusate fully reversed the effects of hyperoxia and rotenone on all model parameters

(Table 3), including $\bar{k}_2$, k_{-2}, and K_{d3}, suggests that the changes in these parameters with rotenone or hyperoxia (Table 3) are likely due to changes in R6G binding kinetics rather than the number of binding sites. Correlations between $\bar{k}_2$, k_{-2}, and K_{d3} and/or between these parameters and other model parameters (Table 4) could also be a factor.

The present study does not provide direct information about the contribution of various cell types to changes in R6G lung uptake and the estimated $\Delta\psi_m$ depolarization due to hyperoxia. The lung consists of 40 different cell types (Dinh et al., 2017)(Kotton & Morrisey, 2014). However endothelial cells would be expected to dominate because of their large surface area and high fraction (~50%) of total cells in normal lungs, and their direct contact with R6G in perfusate (Crapo et al., 1980). Endothelial cells are also considered as the primary and early target of hyperoxia-induced acute lung injury (Crapo et al., 1980)(Audi et al., 2005)(Audi et al., 2008)(Gan et al., 2011). Although the question regarding the contributions of specific cell types to the hyperoxia-induced partial $\Delta\psi_m$ depolarization will be important for future studies, alteration in the lung R6G uptake and estimated $\Delta\psi_m$ as an index of pulmonary mitochondrial dysfunction has functional implications regardless of the lung cell types involved. This could be addressed by measuring the $\Delta\psi_m$ in isolated epithelium and endothelial cells following exposure of the cells to hyperoxic conditions.

Increased vascular permeability is a cardinal feature of clinical ALI (Matthay et al., 2012). Previously, Audi et al. showed that rat exposure to hyperoxia for 48 hours increased the pulmonary endothelial filtration coefficient, K_f, a sensitive measure of endothelial barrier function, by ~ 2 fold (Audi et al., 2016). Bongard et al. showed that inhibiting lung complex I with rotenone, which decreased lung ATP by ~ 60%, increased

K_f by ~ 2.8 fold, and hence established a connection between mitochondrial bioenergetics and K_f(Bongard et al., 2013). Furthermore, the addition of the exogenous quinone CoQ_1 to the isolated rat lung perfusate fully reversed the effect of rotenone on lung ATP and K_f. Further studies are needed to assess the effect of DQ in reversing the effect of hyperoxia on K_f.

Das et al. reported a decrease in the activities of complex I and II in hyperoxia-exposed lung mitochondria. A decrease in complex I and complex II driven oxygen consumption rate (OCR) was observed due to hyperoxia demonstrating a dysfunction of complex II in addition to complex I by producing superoxide (Das, 2013). Therefore, further studies are needed to evaluate the effect of complex I and complex II inhibition to assess their individual effect on the $\Delta\psi_m$ depolarization.

Several different animal models have been used to study acute lung injury, yet there are important and sometimes major differences among animal models in responses to injury. Hyperoxia has been used as a direct and as a secondary injury in animal studies to assess the effect of hyperoxia on mitochondrial bioenergetics.(Matute-Bello et al., 2008) This approach could be utilized in future studies for evaluating the effect of various other models of ALI (eg. LPS treatment, oleic acid) on $\Delta\psi_m$ in intact lungs to determine if this is a common pathway for the pathogenesis of ALI.

In conclusion, this thesis demonstrates our ability to detect and quantify hyperoxia-induced $\Delta\psi_m$ depolarization in intact functioning lungs, and the ability of exogenous quinone compounds such as DQ to fully reverse this depolarization, consistent with hyperoxia-induced decreases in lung complexes I and II activity being the predominant causes for $\Delta\psi_m$ depolarization. This study is the first to measure hyperoxia-

induced $\Delta\psi_m$ depolarization in intact lungs, and to demonstrate the utility of this experimental-computational approach to assess the impact of potential therapies that target mitochondria in intact functioning lungs.

BIBLIOGRAPHY

Adams, J. D., Lauterburg, B. H., & Mitchell, J. R. (1983). Plasma glutathione and glutathione disulfide in the rat: Regulation and response to oxidative stress. The Journal of Pharmacology and Experimental Therapeutics, 227(3), 749–754.

Adrie, C., Bachelet, M., Vayssier-Taussat, M., Russo-Marie, F., Bouchaert, I., Adib-Conquy, M., Cavaillon, J. M., Pinsky, M. R., Dhainaut, J. F., & Polla, B. S. (2001). Mitochondrial membrane potential and apoptosis peripheral blood monocytes in severe human sepsis. American Journal of Respiratory and Critical Care Medicine, 164(3), 389–395. https://doi.org/10.1164/ajrccm.164.3.2009088

al-Mehdi, A. B., Shuman, H., & Fisher, A. B. (1997). Oxidant generation with K(+)-induced depolarization in the isolated perfused lung. Free Radical Biology & Medicine, 23(1), 47–56. https://doi.org/10.1016/s0891-5849(96)00574-6

Alpert, N. M., Guehl, N., Ptaszek, L., Pelletier-Galarneau, M., Ruskin, J., Mansour, M. C., Wooten, D., Ma, C., Takahashi, K., Zhou, Y., Shoup, T. M., Normandin, M. D., & El Fakhri, G. (2018). Quantitative in vivo mapping of myocardial mitochondrial membrane potential. PloS One, 13(1), e0190968. https://doi.org/10.1371/journal.pone.0190968

Aquilano, K., Baldelli, S., & Ciriolo, M. R. (2014). Glutathione: New roles in redox signaling for an old antioxidant. Frontiers in Pharmacology, 5, 196. https://doi.org/10.3389/fphar.2014.00196

Audi, S. H., Bongard, R. D., Dawson, C. A., Siegel, D., Roerig, D. L., & Merker, M. P. (2003). Duroquinone reduction during passage through the pulmonary circulation. American Journal of Physiology. Lung Cellular and Molecular Physiology, 285(5), L1116-1131. https://doi.org/10.1152/ajplung.00185.2003

Audi, S. H., Bongard, R. D., Krenz, G. S., Rickaby, D. A., Haworth, S. T., Eisenhauer, J., Roerig, D. L., & Merker, M. P. (2005). Effect of chronic hyperoxic exposure on duroquinone reduction in adult rat lungs. American Journal of Physiology. Lung Cellular and Molecular Physiology, 289(5), L788-797. https://doi.org/10.1152/ajplung.00064.2005

Audi, S. H., Cammarata, A., Clough, A. V., Dash, R. K., & Jacobs, E. R. (2020). Quantification of mitochondrial membrane potential in the isolated rat lung using rhodamine 6G. Journal of Applied Physiology (Bethesda, Md.: 1985), 128(4), 892–906. https://doi.org/10.1152/japplphysiol.00789.2019

Audi, S. H., Jacobs, E. R., Zhang, X., Camara, A. K. S., Zhao, M., Medhora, M. M., Rizzo, B., & Clough, A. V. (2017). Protection by Inhaled Hydrogen Therapy in a Rat Model of Acute Lung Injury can be Tracked in vivo Using Molecular Imaging. Shock (Augusta, Ga.), 48(4), 467–476. https://doi.org/10.1097/SHK.0000000000000872

Audi, S. H., Merker, M. P., Krenz, G. S., Ahuja, T., Roerig, D. L., & Bongard, R. D. (2008). Coenzyme Q1 redox metabolism during passage through the rat pulmonary circulation and the effect of hyperoxia. Journal of Applied Physiology (Bethesda, Md.: 1985), 105(4), 1114–1126. https://doi.org/10.1152/japplphysiol.00177.2008

Audi, S. H., Clough, A. V., Haworth, S. T., Medhora, M., Ranji, M., Densmore, J. C., & Jacobs, E. R. (2016). 99MTc-Hexamethylpropyleneamine Oxime Imaging for Early Detection of Acute Lung Injury in Rats Exposed to Hyperoxia or Lipopolysaccharide Treatment. Shock (Augusta, Ga.), 46(4), 420–430. https://doi.org/10.1097/SHK.0000000000000605

Bagkos, G., Koufopoulos, K., & Piperi, C. (2014). A new model for mitochondrial membrane potential production and storage. Medical Hypotheses, 83(2), 175–181. https://doi.org/10.1016/j.mehy.2014.05.001

Baracca, A., Sgarbi, G., Solaini, G., & Lenaz, G. (2003). Rhodamine 123 as a probe of mitochondrial membrane potential: Evaluation of proton flux through F0 during ATP synthesis. Biochimica et Biophysica Acta (BBA) - Bioenergetics, 1606(1), 137–146. https://doi.org/10.1016/S0005-2728(03)00110-5

Barrientos, A., & Moraes, C. T. (1999). Titrating the effects of mitochondrial complex I impairment in the cell physiology. The Journal of Biological Chemistry, 274(23), 16188–16197. https://doi.org/10.1074/jbc.274.23.16188

Bassett, D. J., Elbon, C. L., & Reichenbaugh, S. S. (1992). Respiratory activity of lung mitochondria isolated from oxygen-exposed rats. The American Journal of Physiology, 263(4 Pt 1), L439-445. https://doi.org/10.1152/ajplung.1992.263.4.L439

Beyer, A. M., Norwood Toro, L. E., Hughes, W. E., Young, M., Clough, A. V., Gao, F., Medhora, M., Audi, S. H., & Jacobs, E. R. (2021). Autophagy, TERT, and mitochondrial dysfunction in hyperoxia. American Journal of Physiology. Heart and Circulatory Physiology. https://doi.org/10.1152/ajpheart.00166.2021

Block, E. R., & Fisher, A. B. (1977). Depression of serotonin clearance by rat lungs during oxygen exposure. Journal of Applied Physiology: Respiratory, Environmental and Exercise Physiology, 42(1), 33–38. https://doi.org/10.1152/jappl.1977.42.1.33

Bongard, R. D., Townsley, M. I., & Merker, M. P. (2015). The effects of mitochondrial complex I blockade on ATP and permeability in rat pulmonary microvascular endothelial cells in culture (PMVEC) are overcome by coenzyme Q1 (CoQ1). Free Radical Biology & Medicine, 79, 69–77. https://doi.org/10.1016/j.freeradbiomed.2014.09.030

Bongard, R. D., Yan, K., Hoffmann, R. G., Audi, S. H., Zhang, X., Lindemer, B. J., Townsley, M. I., & Merker, M. P. (2013). Depleted energy charge and increased pulmonary endothelial permeability induced by mitochondrial complex I inhibition are mitigated by coenzyme Q1 in the isolated perfused rat lung. Free Radical Biology & Medicine, 65, 1455–1463. https://doi.org/10.1016/j.freeradbiomed.2013.07.040

Bronner, C., & Landry, Y. (1991). The use of the potential-sensitive fluorescent probe bisoxonol in mast cells. Biochimica Et Biophysica Acta, 1070(2), 321–331. https://doi.org/10.1016/0005-2736(91)90073-h

Automatic citation updates are disabled. To see the bibliography, click Refresh in the Zotero tab.

Chan, T. S., Teng, S., Wilson, J. X., Galati, G., Khan, S., & O'Brien, P. J. (2002). Coenzyme Q cytoprotective mechanisms for mitochondrial complex I cytopathies involves NAD(P)H: Quinone oxidoreductase 1(NQO1). Free Radical Research, 36(4), 421–427. https://doi.org/10.1080/10715760290021270

Cloonan, S. M., Kim, K., Esteves, P., Trian, T., & Barnes, P. J. (2020). Mitochondrial dysfunction in lung ageing and disease. European Respiratory Review: An Official Journal of the European Respiratory Society, 29(157), 200165. https://doi.org/10.1183/16000617.0165-2020

Crapo, J. D., Barry, B. E., Foscue, H. A., & Shelburne, J. (1980). Structural and biochemical changes in rat lungs occurring during exposures to lethal and adaptive doses of oxygen. The American Review of Respiratory Disease, 122(1), 123–143. https://doi.org/10.1164/arrd.1980.122.1.123

Das, K. C. (2013). Hyperoxia decreases glycolytic capacity, glycolytic reserve and oxidative phosphorylation in MLE-12 cells and inhibits complex I and II function, but not complex IV in isolated mouse lung mitochondria. PloS One, 8(9), e73358. https://doi.org/10.1371/journal.pone.0073358

Dell'Antone, P., Colonna, R., & Azzone, G. F. (1972). The membrane structure studied with cationic dyes. 1. The binding of cationic dyes to submitochondrial particles and the question of the polarity of the ion-translocation mechanism. European Journal of Biochemistry, 24(3), 553–565. https://doi.org/10.1111/j.1432-1033.1972.tb19718.x

Dinh, P.-U. C., Cores, J., Hensley, M. T., Vandergriff, A. C., Tang, J., Allen, T. A., Caranasos, T. G., Adler, K. B., Lobo, L. J., & Cheng, K. (2017). Derivation of therapeutic lung spheroid cells from minimally invasive transbronchial pulmonary biopsies. Respiratory Research, 18(1), 132. https://doi.org/10.1186/s12931-017-0611-0

Esper, A. M., & Martin, G. S. (2005). Evolution of treatments for patients with acute lung injury. Expert Opinion on Investigational Drugs, 14(5), 633–645. https://doi.org/10.1517/13543784.14.5.633

Fisher, A. B. (1978). Energy status of the rat lung after exposure to elevated PO2. Journal of Applied Physiology: Respiratory, Environmental and Exercise Physiology, 45(1), 56–59. https://doi.org/10.1152/jappl.1978.45.1.56

Fisher, A. B. (1984). Intermediary metabolism of the lung. Environmental Health Perspectives, 55, 149–158.

Fisher, A. B., & Beers, M. F. (2008). Hyperoxia and acute lung injury. American Journal of Physiology - Lung Cellular and Molecular Physiology, 295(6), L1066. https://doi.org/10.1152/ajplung.90486.2008

Galley, H. F. (2011). Oxidative stress and mitochondrial dysfunction in sepsis. British Journal of Anaesthesia, 107(1), 57–64. https://doi.org/10.1093/bja/aer093

Gan, Z., Audi, S. H., Bongard, R. D., Gauthier, K. M., & Merker, M. P. (2011). Quantifying mitochondrial and plasma membrane potentials in intact pulmonary arterial endothelial cells based on extracellular disposition of rhodamine dyes. American Journal of Physiology. Lung Cellular and Molecular Physiology, 300(5), L762-772. https://doi.org/10.1152/ajplung.00334.2010

Gao, L., Laude, K., & Cai, H. (2008). Mitochondrial pathophysiology, reactive oxygen species, and cardiovascular diseases. The Veterinary Clinics of North America. Small Animal Practice, 38(1), 137–155, vi. https://doi.org/10.1016/j.cvsm.2007.10.004

Han, S., & Mallampalli, R. K. (2015). The acute respiratory distress syndrome: From mechanism to translation. Journal of Immunology (Baltimore, Md. : 1950), 194(3), 855–860. https://doi.org/10.4049/jimmunol.1402513

Hough, R. F., Islam, M. N., Gusarova, G. A., Jin, G., Das, S., & Bhattacharya, J. (2019). Endothelial mitochondria determine rapid barrier failure in chemical lung injury. JCI Insight, 4(3), 124329. https://doi.org/10.1172/jci.insight.124329

Johnson, L. V., Walsh, M. L., Bockus, B. J., & Chen, L. B. (1981). Monitoring of relative mitochondrial membrane potential in living cells by fluorescence microscopy. The Journal of Cell Biology, 88(3), 526–535. https://doi.org/10.1083/jcb.88.3.526

Kallet, R. H., & Matthay, M. A. (2013). Hyperoxic Acute Lung Injury. Respiratory Care, 58(1), 123–141. https://doi.org/10.4187/respcare.01963

Kauppinen, R. A., & Hassinen, I. E. (1984). Monitoring of mitochondrial membrane potential in isolated perfused rat heart. The American Journal of Physiology, 247(4 Pt 2), H508-516. https://doi.org/10.1152/ajpheart.1984.247.4.H508

Kellner, M., Noonepalle, S., Lu, Q., Srivastava, A., Zemskov, E., & Black, S. M. (2017). ROS Signaling in the Pathogenesis of Acute Lung Injury (ALI) and Acute Respiratory Distress Syndrome (ARDS). Advances in Experimental Medicine and Biology, 967, 105–137. https://doi.org/10.1007/978-3-319-63245-2_8

Korzeniewski, B. (2015). 'Idealized' State 4 and State 3 in Mitochondria vs. Rest and Work in Skeletal Muscle. PLOS ONE, 10(2), e0117145. https://doi.org/10.1371/journal.pone.0117145

Kotton, D. N., & Morrisey, E. E. (2014). Lung regeneration: Mechanisms, applications and emerging stem cell populations. Nature Medicine, 20(8), 822–832. https://doi.org/10.1038/nm.3642

Laffey, J. G., & Matthay, M. A. (2017). Fifty Years of Research in ARDS. Cell-based Therapy for Acute Respiratory Distress Syndrome. Biology and Potential Therapeutic Value. American Journal of Respiratory and Critical Care Medicine, 196(3), 266–273. https://doi.org/10.1164/rccm.201701-0107CP

Lanza, I. R., & Nair, K. S. (2009). Functional assessment of isolated mitochondria in vitro. Methods in Enzymology, 457, 349–372. https://doi.org/10.1016/S0076-6879(09)05020-4

Levitt, J. E., & Matthay, M. A. (2012). Clinical review: Early treatment of acute lung injury--paradigm shift toward prevention and treatment prior to respiratory failure. Critical Care (London, England), 16(3), 223. https://doi.org/10.1186/cc11144

Liu, X., & Chen, Z. (2017). The pathophysiological role of mitochondrial oxidative stress in lung diseases. Journal of Translational Medicine, 15(1), 207. https://doi.org/10.1186/s12967-017-1306-5

Ma, K., Patel, K., Naddour, M., Virani, A., Adurty, R., AlhajHusain, A., & Cheema, T. (2019). Acute Respiratory Distress Syndrome Novel Therapies. Critical Care Nursing Quarterly, 42(4), 411–416. https://doi.org/10.1097/CNQ.0000000000000281

Matthay, M. A., Ware, L. B., & Zimmerman, G. A. (2012). The acute respiratory distress syndrome. The Journal of Clinical Investigation, 122(8), 2731–2740. https://doi.org/10.1172/JCI60331

Matthay, M. A., Zemans, R. L., Zimmerman, G. A., Arabi, Y. M., Beitler, J. R., Mercat, A., Herridge, M., Randolph, A. G., & Calfee, C. S. (2019). Acute respiratory

distress syndrome. Nature Reviews. Disease Primers, 5(1), 18. https://doi.org/10.1038/s41572-019-0069-0

Matthay, M. A., Zimmerman, G. A., Esmon, C., Bhattacharya, J., Coller, B., Doerschuk, C. M., Floros, J., Gimbrone, M. A., Hoffman, E., Hubmayr, R. D., Leppert, M., Matalon, S., Munford, R., Parsons, P., Slutsky, A. S., Tracey, K. J., Ward, P., Gail, D. B., & Harabin, A. L. (2003). Future research directions in acute lung injury: Summary of a National Heart, Lung, and Blood Institute working group. American Journal of Respiratory and Critical Care Medicine, 167(7), 1027–1035. https://doi.org/10.1164/rccm.200208-966WS

Matute-Bello, G., Frevert, C. W., & Martin, T. R. (2008). Animal models of acute lung injury. American Journal of Physiology. Lung Cellular and Molecular Physiology, 295(3), L379-399. https://doi.org/10.1152/ajplung.00010.2008

Merker, M. P., Audi, S. H., Bongard, R. D., Lindemer, B. J., & Krenz, G. S. (2006). Influence of pulmonary arterial endothelial cells on quinone redox status: Effect of hyperoxia-induced NAD(P)H:quinone oxidoreductase 1. American Journal of Physiology. Lung Cellular and Molecular Physiology, 290(3), L607-619. https://doi.org/10.1152/ajplung.00302.2005

Merker, M. P., Audi, S. H., Lindemer, B. J., Krenz, G. S., & Bongard, R. D. (2007). Role of mitochondrial electron transport complex I in coenzyme Q1 reduction by intact pulmonary arterial endothelial cells and the effect of hyperoxia. American Journal of Physiology. Lung Cellular and Molecular Physiology, 293(3), L809-819. https://doi.org/10.1152/ajplung.00448.2006

Merker, M. P., Bongard, R. D., Krenz, G. S., Zhao, H., Fernandes, V. S., Kalyanaraman, B., Hogg, N., & Audi, S. H. (2004). Impact of pulmonary arterial endothelial cells on duroquinone redox status. Free Radical Biology & Medicine, 37(1), 86–103. https://doi.org/10.1016/j.freeradbiomed.2004.02.078

Mittal, M., Siddiqui, M. R., Tran, K., Reddy, S. P., & Malik, A. B. (2014). Reactive oxygen species in inflammation and tissue injury. Antioxidants & Redox Signaling, 20(7), 1126–1167. https://doi.org/10.1089/ars.2012.5149

Neergheen, V., Chalasani, A., Wainwright, L., Yubero, D., Montero, R., Artuch, R., & Hargreaves, I. (2017). Coenzyme Q 10 in the Treatment of Mitochondrial Disease. Journal of Inborn Errors of Metabolism and Screening, 5, 232640981770777. https://doi.org/10.1177/2326409817707771

Perry, S. W., Norman, J. P., Barbieri, J., Brown, E. B., & Gelbard, H. A. (2011). Mitochondrial membrane potential probes and the proton gradient: A practical usage guide. BioTechniques, 50(2), 98–115. https://doi.org/10.2144/000113610

Pizzino, G., Irrera, N., Cucinotta, M., Pallio, G., Mannino, F., Arcoraci, V., Squadrito, F., Altavilla, D., & Bitto, A. (2017). Oxidative Stress: Harms and Benefits for Human Health. Oxidative Medicine and Cellular Longevity, 2017, 8416763. https://doi.org/10.1155/2017/8416763

Presnell, C. E., Bhatti, G., Numan, L. S., Lerche, M., Alkhateeb, S. K., Ghalib, M., Shammaa, M., & Kavdia, M. (2013). Computational insights into the role of glutathione in oxidative stress. Current Neurovascular Research, 10(2), 185–194. https://doi.org/10.2174/1567202611310020011

Sakamuru, S., Attene-Ramos, M. S., & Xia, M. (2016). Mitochondrial Membrane Potential Assay. Methods in Molecular Biology (Clifton, N.J.), 1473, 17–22. https://doi.org/10.1007/978-1-4939-6346-1_2

Scaduto, R. C., & Grotyohann, L. W. (1999). Measurement of mitochondrial membrane potential using fluorescent rhodamine derivatives. Biophysical Journal, 76(1 Pt 1), 469–477.

Schumacker, P. T., Gillespie, M. N., Nakahira, K., Choi, A. M. K., Crouser, E. D., Piantadosi, C. A., & Bhattacharya, J. (2014). Mitochondria in lung biology and pathology: More than just a powerhouse. American Journal of Physiology. Lung Cellular and Molecular Physiology, 306(11), L962-974. https://doi.org/10.1152/ajplung.00073.2014

Sepehr, R., Audi, S. H., Staniszewski, K. S., Haworth, S. T., Jacobs, E. R., & Ranji, M. (2013). Novel Flurometric Tool to Assess Mitochondrial Redox State of Isolated Perfused Rat Lungs after Exposure to Hyperoxia. IEEE Journal of Translational Engineering in Health and Medicine, 1, 1500210. https://doi.org/10.1109/JTEHM.2013.2285916

Sood, B., & Keenaghan, M. (2021). Coenzyme Q10. In StatPearls. StatPearls Publishing. http://www.ncbi.nlm.nih.gov/books/NBK531491/

Ten, V. S., & Ratner, V. (2020). Mitochondrial bioenergetics and pulmonary dysfunction: Current progress and future directions. Paediatric Respiratory Reviews, 34, 37–45. https://doi.org/10.1016/j.prrv.2019.04.001

Wan, B., Doumen, C., Duszynski, J., Salama, G., Vary, T. C., & LaNoue, K. F. (1993). Effects of cardiac work on electrical potential gradient across mitochondrial membrane in perfused rat hearts. American Journal of Physiology-Heart and Circulatory Physiology, 265(2), H453–H460. https://doi.org/10.1152/ajpheart.1993.265.2.H453

Wolken, G. G., & Arriaga, E. A. (2014). Simultaneous measurement of individual mitochondrial membrane potential and electrophoretic mobility by capillary

electrophoresis. Analytical Chemistry, 86(9), 4217–4226. https://doi.org/10.1021/ac403849x

Zhang, Q., Matsuzaki, I., Chatterjee, S., & Fisher, A. B. (2005). Activation of endothelial NADPH oxidase during normoxic lung ischemia is KATP channel dependent. American Journal of Physiology-Lung Cellular and Molecular Physiology, 289(6), L954–L961. https://doi.org/10.1152/ajplung.00210.2005

Zorov, D. B., Juhaszova, M., & Sollott, S. J. (2014). Mitochondrial reactive oxygen species (ROS) and ROS-induced ROS release. Physiological Reviews, 94(3), 909–950. https://doi.org/10.1152/physrev.00026.2013

Zorova, L. D., Popkov, V. A., Plotnikov, E. Y., Silachev, D. N., Pevzner, I. B., Jankauskas, S. S., Babenko, V. A., Zorov, S. D., Balakireva, A. V., Juhaszova, M., Sollott, S. J., & Zorov, D. B. (2018). Mitochondrial membrane potential. Analytical Biochemistry, 552, 50–59. https://doi.org/10.1016/j.ab.2017.07.009

APPENDIX I

Protocol for R6G Experiment

Materials required

- Prepare perfusate (450 ml per lung)
- Eppendorf 1.7ml
  - Phase1 – 11*2
  - Phase 2 – 6*2
  - Phase 3 – 12*2
  - Verapamil - 3
  - FCCP- 1
  - Rotenone -3
  - Duroquinone – 1
  - GSH - 1
- Sharpie to label
- Two small bottles to prepare R6G stock 1 and 2
- Aluminum foil
- Weighing paper
- Pipettes
  - P1000 – Standard curve,
    - R6G Stock,
    - Adding R6G to perfusate in phase I
    - Adding DMSO to Duroquinone
    - Transferring samples from eppendorfs to cuvette
  - P200 – Adding DMSO to Rotenone
    - Adding Verapamil to perfusate
    - Adding FCCP to perfusate
  - P100 – Adding stock 1 R6G to stock 2,
    - Adding rotenone to perfusate in phase I, II, III
    - Adding Duroquinone to perfusate in phase II and phase III
  - P10 - Adding R6G to perfusate for standard curve
- Pipette tips (P1000, P200, P100, P10)
- 5ml tubes - 6
- DH_2O
- R6G dye – 1mg/ml of DH_2O
- Verapamil – prepare three Eppendorf's for three phases and calculate how much is required per volume of perfusate
- Rotenone
- Duroquinone
- FCCP for phase III
- Timer
- Spatula - 2
- Mixer
- Three beakers for perfusate for the three phases

- Pressure calibrator
- Big syringe with tube to remove liquid from reservoir
- Graduated cylinders
- Cuvettes
- Centrifuge
- PTI System

Before experiment

- Prepare 450ml of perfusate
- Take eppendorf holders and label them as:
    1. Standard curve + verapamil (2*6 1.7ml for each concentration)
    2. Phase 1
    3. Phase 2
    4. Phase 3
- Label the standard curve eppendorfs with the following concentrations
    1. 0
    2. 0.03
    3. 0.06
    4. 0.125
    5. 0.25
    6. 0.5
- Prepare eppendorfs for verapamil, rotenone and Duroquinone
- Label the phase 1 according to the time at which the samples have to be taken:

(Bg, 0s, 40s, 80s, 120s, 3min, 4min, 5min, 7min, 9 min,10min)

- Label the phase 2 according to the time at which the samples have to be taken:

(0s, 1min, 2min, 3min, 4min, 5min)

- Label the phase 3 according to the time at which the samples have to be taken:

(0s ,20s, 40s,60s, 80s,100s, 120s, 3min, 4min,5min, 6min,7min)

- Set the centrifuge to 4°C for 1min at 10.5x1000 rpm
- Turn on the incubator and set to 37°C
- Turn on the PTI system at least 30 min before the start of the experiment

R6G stock

- For stock 1, take 1 small bottle and cover it in aluminum foil since R6G is sensitive to light
- Label it as 1
- Weigh 1mg = 0.001g of R6G dye using the weighing paper and add it to stock 1 bottle
- Add 1ml of DH_2O to stock 1 and mix completely to get a concentration of 2.09mM
- For stock 2, take another bottle and cover with aluminum foil and label as 2
- Using P1000 pipette add 1.96ml of DH_2O and P100 to add 40 µL of stock 1 to stock 2 and mix completely to get a concentration of 41.8µM
- Keep the stocks in a dark place

For verapamil

- Take 3 eppendorfs and cover with aluminum foil and label as phase I, II, III

- Weigh 10mg of verapamil for 200ml of perfusate and store it in the eppendorf labeled phase I
- Weigh 5mg of verapamil for 100ml of perfusate and store it in the eppendorf labeled phase II
- Weigh 5mg of verapamil for 100ml of perfusate and store it in the eppendorf labeled phase III

Rotenone stock

Concentration = 100µM

5mg rotenone + 0.125ml DMSO = 100µM of rotenone stock per tube

- Take 3 eppendorfs and cover with an aluminum foil and label with a sharpie as R1, R2 and R3.
- Weigh 5mg of rotenone for each phase and add it to the eppendorf and place in the dark till experiment.
- Just before the start of a phase, add 0.125ml of DMSO to the eppendorf containing Rotenone for that respective phase and place on the mixer to mix well till it is completely in solution.
- For 200ml, add 80µL of rotenone stock to 200ml perfusate = 40µM
- For 100ml, add 40µL of rotenone stock to 100ml perfusate= 40µM

Duroquinone stock

Concentration = 187.5µM

15mg DQ + 0.5mL DMSO = 187.5µM

- Take 1 eppendorf and cover with an aluminum foil and label with a sharpie as DQ
- Weigh 15mg of DQ and add it to the eppendorf and place in the dark till experiment.
- Just before the start of a phase, add 0.5ml of DMSO to the eppendorf containing DQ and place on the mixer to mix well till it is completely in solution.
- For 200ml, add 107µL of stock to 200ml perfusate for 100µM final conc
- For 100ml, add 53.3µL of stock to 100ml perfusate for 100µM final conc

GSH stock

Concentration = 100µM

15.4mg GSH + 0.5mL DH_2O= 100µM

- Take 1 eppendorf and cover with an aluminum foil and label with a sharpie as GSH
- Weigh 15.4mg of GSH and add it to the eppendorf and place in the dark till experiment.
- Just before the start of a phase, add 0.5ml of DH_2O to the eppendorf containing GSH and place on the mixer to mix well till it is completely in solution.
- For 200ml, add 32µL of stock to 200ml perfusate for 16µM final conc
- For 100ml, add 16µL of stock to 100ml perfusate for 16µM final conc

R6G PROTOCOL

Phase I

- Take a beaker with 200ml of perfusate and add the verapamil for phase 1 and mix well

- Take 120ml from this 200ml of perfusate and add 0.7177ml of R6G dye from stock 2 to get a concentration of 0.25µM
- Pipette 2ml from the perfusate containing the dye and take a measurement using the PTI system to ensure the concentration of the dye is within range
- The remaining 80ml of perfusate with verapamil is used to wash the lung for 3 min.
- Take a background sample (bg) in the two 1.7ml eppendorfs from the perfusate without the dye
- Drain the perfusate without R6G from the reservoir
- Add 50mL of the perfusate with R6G and add more eventually when collecting samples to avoid the reservoir from emptying and air entering
- Take 0s sample and then turn on the pump
- Take samples at 40s, 80s, 120s, 3min, 5min, 7min, 9 min,10min (using 2 1.7ml eppendorfs per sample)
- The flow rate is at 10ml/min, so the samples are taken for 12 seconds each
- The samples are collected 6 seconds before and 6 seconds after the mentioned sample time
- The flow is stopped, and the reservoir is washed with perfusate for 3min before the next phase

Phase II

- Before the completion of phase I, take a beaker and fill 100mL of perfusate
- Add the verapamil from the eppendorf labeled as phase II
- Mix well and keep ready
- Before turning the pump back on, take 0s samples
- Turn the pump on and take samples at 1min, 2min, 3min, 4min, 5min (using 2 1.7ml eppendorfs per sample time)
- Stop the flow and wash the reservoir

Phase III

- Before the completion of phase II, take a beaker and fill 100mL of perfusate and add the verapamil
- Using graduated cylinder, measure 75 ml of perfusate with verapamil and transfer to another beaker
- Add the FCCP from the eppendorf to the perfusate
- Mix well and keep ready
- Before turning the pump back on, take 0s samples
- Turn the pump on and take samples at 20s, 40s,60s, 80s,100s, 120s, 3min, 4min,5min, 6min,7min (using 2 1.7ml eppendorfs per sample time)

Centrifugation

- Turn the lights off before centrifugation
- Centrifuge the samples from each phase at 10.5x1000 rpm @ 4°C for 1min
- Add each sample time from each phase into a cuvette and measure for fluorescence
- Make sure to use one cuvette per sample time per phase

Fluorescence reading

- Switch on the optical imaging system and computer as per protocol
- Open the Felix software
- Click ‘Setup’ -> Time based acquisition
- Click on acquisition settings tab
- Set emission: 565nm and excitation: 525nm
- Change the acquisition time to 300s
- Set the excitation window to 1.875nm by adjusting the two knobs (1 complete rotation is 2.5nm)
- Click ‘Start’ to start acquisition of data

Standard Curve

- Take 6 5ml tubes for dilution of R6G
- Label them according to their concentrations (0,0.03,0.06,0.125,0.25,0.5)
- Using the P1000 pipette, add 4.5ml of perfusate+verapamil to the tube labeled 0.05
- Fill the remaining tubes with 2.25ml of perfusate+verapamil
- Tube 0.05µM: Add 53.8 µL to tube 0.05 and mix
  Pipette 2x1ml from the tube to the eppendorfs
  Pipette 2.25ml to tube 0.25
- Tube 0.25µM: Mix well
  Pipette 2x1ml from the tube to the eppendorfs
  Pipette 2.25ml to tube 0.125
- Tube 0.125µM: Mix well
  Pipette 2x1ml from the tube to the eppendorfs
  Pipette 2.25ml to tube 0.06
- Tube 0.06µM: Mix well
  Pipette 2x1ml from the tube to the eppendorfs
  Pipette 2.25ml to tube 0.03
- Tube 0.03µM: Mix well
  Pipette 2x1ml from the tube to the eppendorfs
- Tube 0µM: Pipette 2x1ml from the tube to the eppendorfs containing only perfusate+verapamil without r6g
- Add each sample from each concentration into a cuvette and measure for fluorescence
- Make sure to use one cuvette per sample concentration

APPENDIX II
MATLAB CODE

Simulation Code

1. r6g_single_pass_parameters.m

```
% Function: simulate concentration of R6G with given parameters
% Input: none
% Output: a datafile containing simulated data

close all
clc
global deltap F deltam_un

% Values for model parameters
vmaxkm = 0.0; % Kpgp Rate (ml/min)
k2_bar = 6.90;% rate constant for binding within the cytoplasm region
kminus2 = 0.178;%Dissociation rate constant within the cytoplasm region
kd3 = 0.018;%Dissociation constant in the mitochondria region
ps2 = 1.07; %Permeability-Surface area product across mitochondrial membrane
deltam = -131.2; % Mitochondrial membrane potential (mV)
deltam_un = -0.1; % Mitochondrial membrane potential after adding FCCP (mV)
ps1 = 46.54; %Permeability-Surface area product across plasma membrane
deltap = -43; %Plasma membrane potential(mV)
F = 10; %Pump flow(ml/min)

% Initial concentrations
Ce_bar = 0; %initial vascular R6G concentration (uM)
Cc = 0;     %initial tissue R6G concentration (uM)
Cm = 0;     %initial mitochondrial R6G concentration (uM)
CcBc = 0;   %intial bound r6g cytoplasm concentration (uM)
Ctub1 = 0;  %intial tubing r6g concentration (uM)

%Parameters that are being optimized to their initial points;
y(1) = k2_bar;
y(2) = kminus2;
y(3) = kd3;
y(4) = deltam;
y(5) = ps1;
y_value= [k2_bar, kminus2 , kd3, deltam, ps1 ];

%solving ODE
tspan = [0:0.1:22]';
y0 = [Ctub1 Ce_bar Cc Cm CcBc];  % concentrations (uM)

[tfinal,xfinal] = ode45(@r6g_odes1, tspan, y0, [], y_value); %calling to ode
```

```
%plotting the model
plot(tspan, xfinal(:,2),'linewidth',1);
xlabel('Time (minutes)');
ylabel('Concentration (uM)');

% to write data to a file
file = 'simulation.txt';
write = fopen(file, 'w');

for i=1:length(tspan)
fprintf(write,'%f %f\n', tspan(i), xfinal(i,2));
end
fclose(write);
```

2. r6g_single_pass_odes.m

```
% Function: calculate concentration of R6G at a specific time with given parameters
% Input: time: sampling time
% y: concentrations of R6G in tubing region, extravascular region, vascular region, and
        mitochondrial region
% Output: Concentration of R6G

function [ dC_dt ] = r6g_odes1(tspan,c, y ,a)
dC_dt = zeros(5,1);


global deltap F deltam_un

% Value of parameters
Ve = 0.85; %Extravascular volume (ml)
Vc = 1.0;  %Cytoplasm volume (ml)
Vm = 0.02*Vc; % mitochondrial volume (ml)
Vtub = 4; % tube volume (ml)
alpha = 0.0374158; %ZF/RT, where Z is the valency of the ions, F is Faraday's constant
(9.684 x 104 C/ mol), R is the gas constant (8.135 J/K*mol), and T is the absolute
temperature in K (273 + temp in Celcius). (mV-1)
Be = 0.5; %BSA concentration (uM)
kd1 = 0.32; %Dissociation constant in the vascular region
vmaxkm=0;
ps2 = 1.07;%  Permeability-Surface area product across mitochondrial membrane


%parameters
k2_bar = y(1);
kminus2 = y(2);
```

```
kd3 = y(3);
deltam = y(4);
ps1 = y(5);

% calculate the apparent volume
Vm_app = Vm*(1+(1/kd3)); % apparent volume of the mitochondria extravascular
region

% Concentration of initial R6G based on phase
if tspan >= 0 && tspan <= (t-11.6) %loading phase
Cin = 0.25;

elseif tspan > (t-11.6) && tspan <(t-6.6) % wash phase
Cin = 0;

elseif tspan >= (t-6.6) %uncoupler phase
Cin = 0;
deltam = deltam_un; %Mitochondrial membrane potential with uncoupler (mV)
end


% Free concentration of r6g within the vascular region
Ce = (c(2)/(1+(Be)/(kd1))); %nmol/mL

%  flux values
J1 = -((alpha*ps1*deltap)/(exp(-alpha*deltap)-1))*(exp(-alpha*deltap)*Ce-c(3));
%(nmol/min)
J2 = -((alpha*ps2*deltam)/(exp(-alpha*deltam)-1))*(exp(-alpha*deltam)*c(3)-c(4));
%(nmol/min)

% ODEs
dC_dt(1,1) = (1.0/(Vtub))*F*(Cin-c(1)); % tubing region
dC_dt(2,1) = (1/Ve)*(-J1+vmaxkm*c(3)+F*(c(1)-c(2))); % vascular region
dC_dt(3,1) = kminus2*c(5)-k2_bar*c(3)+(1/Vc)*(J1-J2-vmaxkm*c(3)); % cytoplasm
region free
dC_dt(4,1) = (1/Vm_app)*(J2); % mitochondrial region
dC_dt(5,1) = k2_bar*c(3)-kminus2*c(5); % cytoplasm region bound
end
```

Optimization code

3. **data_fit.m**

```
% Function: Find the optimized value for the parameters
% Input: experimental data
% Output: optimized value of parameters
% Format of input data:
```

```
% 1st column: sampling time
% 2nd column: R6G concentration at corresponding sampling time

clear all;
close all;
clc;
global deltap F deltam_un

% load the data file to be fit
y = load (normoxia mean.txt');
time = y(:,1);
data = y(:,2);
timedata = [time];
data = [data];


% Initial value for unknown parameters
k2_bar = 7;% rate constant for binding within the cytoplasm region
deltam = -140.6; % Mitochondrial membrane potential (mV)
deltam_un = 0.1; % Mitochondrial membrane potential after adding FCCP (mV)
ps1 = 46.69; %dye permeability-surface area product across plasma membrane (ml/min)
kminus2 = 0.172;%Dissociation rate constant within the cytoplasm region
kd3 = 0.016;%Dissociation constant in the mitochondria region

%Fixed parameter values
deltap = -43; %Plasma membrane potential (mV)
F = 10; %Flow (ml/min)
vmaxkm = 0.0; % Kpgp Rate (ml/min)
ps2 = 1.12 ;%  Permeability-Surface area product across mitochondrial membrane

% Defining the parameters which will be estimated
param = [k2_bar, kminus2, kd3, deltam, ps1 ];

% defining the lower and upper boundary values of the estimated parameter values
lb = [-200 -200 -200 -200 -200];% lower bound
ub = [200 200 200 200 200]; % upper bound

% fitting model to input data and find out the optimized values for parameters using
lsqcurvefit
[x, ssd, residual, ef, outt,lambda, jacobian] = lsqcurvefit(@r6g_par, param, timedata,
data, lb,ub, []);

%parameters
parameter(1,1) = x(1);
parameter(1,2) = x(2);
parameter(1,3) = x(3);
```

```
parameter(1,4) = x(4);
parameter(1,5) = x(5);

% Display the value of model parameters
fprintf(' k2_bar = %f \n', x(1)); % Display value of k2_bar
fprintf(' kminus2 = %f\n', x(2)); % Display value of kminus2
fprintf(' kd3 = %f\n', x(3)); % Display value of kd3
fprintf(' deltam = %f\n', x(4)); % Display value of deltam
fprintf(' ps1 = %f\n', x(5)); % Display value of ps1

% model_fit = odes(timedata,y,parameter);
model_fit = data+residual;

%Plot the data and the model fit
plot(timedata,data,'ro');
hold on
plot(timedata, model_fit,'b','LineWidth',0.85);
xticks(0:22);
hold off;
legend('Normoxia data','Model fit ');
xlim([0 22]);
ylim([0 0.18]);
xlabel('Time(min)');
ylabel('R6G Venous effluent Concentration (uM)')

%correlation matrix
NP = length(param);
h = inv(jacobian'*jacobian);
for i = 1:NP;
for j = 1:NP;
cc(i,j) = h(i,j)/((h(i,i)*h(j,j))^0.5);
end
end
full(cc)

%confidence intervals (95% confidence, alpha = 0.05)
s_2 = ssd/(length(data) - NP);
for i = 1:NP;
seb(i) = ((s_2)^0.5)*(h(i,i)^0.5);
end
alpha = 0.05;
tt_dis = - tinv(alpha/2, length(data) - length(param)); % tinv is the Student's t inverse
cumulative

%distribution function
seb = seb.*tt_dis;
```

```
seb;
%%%%%%%%
```

4. r6g_odes.m

```
% Function: calculate concentration of R6G at a specific time with given parameters
        based on rhodamine distribution model
% Input: time: sampling time
% y: concentrations of R6G in tubing region, extravascular region, vascular region and
        mitochondrial region
% Output: Concentration of R6G

function [ dy ] = r6g_odes(timedata,y,x)

%create vector of zeros
dy = zeros(5,1);

global deltap F deltam_un

% Value of parameters
Ve = 0.85; %vascular volume (ml)
Vc = 1;  %lung tissue volume (ml)
Vm = 0.02*Vc; % mitochondrial volume (ml)
Vtub = 4; % tube volume (ml)
alpha = 0.0374158; %ZF/RT, constant dependent on the universal gas constant (R),
Faraday constant (F), R6G valence (Z) , and absolute temperature (T)
Be = 0.5; %BSA concentration (uM)
kd1 = 0.32; % k-1/k1, Dissociation constant in the vascular region (umol-1*min-1)
vmaxkm = 0; % Kpgp rate (ml/min)
ps2 = 1.12;%  Permeability-Surface area product across mitochondrial membrane


% Estimate Parameter values
k2_bar = x(1);
kminus2 = x(2);
kd3 = x(3);
deltam = x(4);
ps1 = x(5);

% calculate apparent volume
V3 = Vm*(1+(1/kd3)); %Apparent mitochondrial volume (ml)

% final time point
t = 22;

% Concentration of R6G based on phase
```

```
if timedata >= 0 && timedata <= (t-11.6) %loading phase
Cin = 0.25; % R6g Concentration

elseif timedata > (t-11.6) && timedata <(t-6.6) % wash phase
Cin = 0;% R6g Concentration

elseif timedata >= (t-6.6) %uncoupler phase
Cin = 0;% R6g Concentration
deltam = deltam_un; %Mitochondrial membrane potential with uncoupler (mV)
end

%Concentration of r6g in the vascular region
Ce = (y(2)/(1+(Be)/(kd1)));

% Flux values
J1 = -((alpha*ps1*deltap)/(exp(-alpha*deltap)-1))*(exp(-alpha*deltap)*Ce-y(3)); %Dye
flux across plasma membrane (nmol/min)
J2 = -((alpha*ps2*deltam)/(exp(-alpha*deltam)-1))*(exp(-alpha*deltam)*y(3)-y(4));
%Dye flux across mitochondrial membrane (nmol/min)

dy(1,1) = (1.0/(Vtub))*F*(Cin-y(1)); % tubing region
dy(2,1) = (1/Ve)*(-J1+vmaxkm*y(3)+F*(y(1)-y(2))); % extracellular/vascular region
units = nmol/mL*min
dy(3,1) = kminus2*y(5)-k2_bar*y(3)+(1/Vc)*(J1-J2-vmaxkm*y(3)); % cytoplasm region
free
dy(4,1) = (1/V3)*(J2); % mitochondrial region units = nmol/mL*min
dy(5,1) = k2_bar*y(3)-kminus2*y(5); % cytoplasm region bound

end
```

5. r6g_par.m

```
% Function: calculate concentration of R6G with given parameters
% Input: y: given parameters
% Output: An array of concentration of R6G

function output = r6g_par(x, timedata)

global deltap F deltam_un

% Set parameters that are being optimized to their initial points;
k2_bar = x(1);
kminus2 = x(2);
kd3 = x(3);
deltam = x(4);
ps1 = x(5);
```

```
parameter_values = [k2_bar,kminus2,  kd3, deltam, ps1];

%Initial conditions for ODE
Ce_bar = 0; %initial vascular R6G concentration (uM)
Cc = 0;     %initial tissue R6G concentration (uM)
Cm = 0;     %initial mitochondrial R6G concentration (uM)
CcBc = 0;   %intial bound r6g cytoplasm concentration (uM)
Ctub1 = 0;  %intial tubing r6g concentration (uM)
x0 = [Ctub1 Ce_bar Cc Cm CcBc];

% Calling ODE function
[T,Y] = ode45(@odes, timedata, x0, [], parameter_values);
output = Y(:,2);
```